European Journal of Medicinal Chemistry 260 (2023) 115756

Contents lists available at ScienceDirect

European Journal of Medicinal Chemistry

journal homepage: www.elsevier.com/locate/ejmech

Research paper

Hydrophobicity modulation *via* the substituents at positions 2 and 4 of 1,3,5-triazine to enhance therapeutic ability against Alzheimer's disease for potent serotonin 5-HT$_6$R agents

Sylwia Sudoł-Tałaj [a,b], Katarzyna Kucwaj-Brysz [a], Sabina Podlewska [c], Rafał Kurczab [c], Grzegorz Satała [c], Barbara Mordyl [d], Monika Głuch-Lutwin [d], Natalia Wilczyńska-Zawal [e], Magdalena Jastrzębska-Więsek [e], Kinga Czarnota-Łydka [a,b], Kinga Kurowska [a], Monika Kubacka [f], Ewa Żesławska [g], Wojciech Nitek [h], Agnieszka Olejarz-Maciej [a], Agata Doroz-Płonka [a], Anna Partyka [e], Gniewomir Latacz [a], Anna Wesołowska [e], Jadwiga Handzlik [a,*]

[a] Department of Technology and Biotechnology of Drugs, Faculty of Pharmacy, Jagiellonian University, Medical College, Medyczna 9, PL 30-688, Kraków, Poland
[b] Doctoral School of Medical and Health Sciences, Jagiellonian University Medical College, Św. Łazarza 16, PL 31-530, Kraków, Poland
[c] Maj Institute of Pharmacology, Polish Academy of Sciences, Department of Medicinal Chemistry, Smętna 12, PL 31-343, Kraków, Poland
[d] Department of Pharmacobiology, Faculty of Pharmacy, Jagiellonian University, Medical College, Medyczna 9, PL 30-688, Kraków, Poland
[e] Department of Clinical Pharmacy, Faculty of Pharmacy, Jagiellonian University, Medical College, Medyczna 9, PL 30-688, Kraków, Poland
[f] Department of Pharmacodynamics, Faculty of Pharmacy, Jagiellonian University, Medical College, Medyczna 9, PL 30-688, Kraków, Poland
[g] Institute of Biology and Earth Sciences, Pedagogical University of Krakow, Podchorążych 2, PL 30-084, Kraków, Poland
[h] Faculty of Chemistry, Jagiellonian University, Gronostajowa 2, PL 30-387, Kraków, Poland

ARTICLE INFO

Keywords:
5-HT$_6$ serotonin receptors
1,3,5-triazine
molecular modelling

ABSTRACT

Alzheimer's disease (AD), a neurodegenerative disorder with a complex aetiology, is the most common memory dysfunction particularly affecting the elderly. Various protein targets have been classified to be involved in the AD treatment, including 5-HT$_6$ receptor (5-HT$_6$R). So far, the 5-HT$_6$R ligands obtained by our research group have become a good basis for hydrophobicity modulation to give a chance for more effective action toward AD by additional influence on target enzymes, e.g. cyclin-dependent kinase 5 (CDK5). In the search for 5-HT$_6$R agents with additional inhibitory action on the enzyme, a series of 25 new 1,3,5-triazines (**7-31**) as modifications of lead, *4-[1-(2,5-dichlorophenoxy)propyl]-6-(4-methylpiperazin-1-yl)-1,3,5-triazine-2-amine* (**6**), was rationally designed. Molecular modelling, synthesis, crystallographic studies, *in vitro* biological assays and behavioral studies *in vivo* were performed. The new triazines showed high affinity (K_i < 100 nM) and selectivity for 5-HT$_6$R. The most effective one, *4-[1-(2,5-difluorophenoxy)propyl]-6-(4-methylpiperazin-1-yl)-1,3,5-triazine-2-amine* (**8**), exhibited the strong antagonistic action towards 5-HT$_6$R (K_i = 5 nM, pK_b = 8.16), had an impact on the memory processes in the Novel Object Recognition test and displayed anxiolytic-like activity in the Elevated Plus Maze test in rats. Moreover, it had the antiplatelet effect as well as very good permeability (PAMPA model), high metabolic stability (RLMs) and satisfactory safety *in vitro*. Although the CDK5 inhibitory effects *in vitro* for the tested compounds (**8**, **10**, **14**, **18**, **26-31**) missed the potency expected from *in silico* simulations, the novel antagonist (**8**) with a very satisfying pharmacological and ADMET profile can serve as a new lead structure in further searches for innovative therapy against AD with accompanying symptoms.

1. Introduction

Alzheimer's disease (AD) is a complex central nervous system (CNS) disorder involving a number of signaling pathways [1,2]. Recently, after no breakthrough in the treatment of this disease for over 20 years, two new biological drugs against AD have been approved by FDA -

* Corresponding author.
E-mail address: j.handzlik@uj.edu.pl (J. Handzlik).

https://doi.org/10.1016/j.ejmech.2023.115756
Received 1 April 2023; Received in revised form 7 August 2023; Accepted 23 August 2023
Available online 24 August 2023

aducanumab (in 2021 [3]) and lecanemab (in 2023 [4]), both of which are monoclonal antibodies. The fact that therapies with these drugs are extremely expensive, and that the primary therapeutic targets of the latest synthetic new molecular entities (NMEs) are still cholinesterases [5], reinforces the compelling need to look for synthetic drugs that offer a chance for accessibility for each patient. Due to the composite aetiology, design of multifunctional molecules, which combine the activity *via* two or more potential AD targets, might be the solution for development of an effective AD therapy. Thus, important AD-related targets, including enzymes and G-protein coupled receptors (GPCRs), gain increasing research attention. As it comes to enzymes, monoamine oxidase B (MAO-B) has been widely explored in the search for new drugs against the neurodegenerative diseases such as AD [6–8]. The MAO-B enzyme found in the brain and peripheral tissues plays an important role in the deamination of biogenic amines and therefore the regulation of neurotransmitter levels [9]. It is still under consideration whether MAO-B inhibitors are effective in the AD treatment. Neuroprotective mechanisms mediated by cyclin-dependent kinase 5 (CDK5) inhibition seem to be also interesting approach leading to AD therapy. The role of this enzyme in AD pathology has been proved by various lines of evidence [10–14]. The kinase CDK5, restricted to neuronal cells, contributes significantly to various important processes of the nervous system, *i.e.*: regulation of synaptic plasticity, release of neurotransmitters and neurite proliferation [15]. Complex CDK5/p25 shows an expanded level of tau phosphorylation, which is the main component of neurofibrillary tangles (NFTs) found in AD patients' brain [16,17].

Among GPCRs, the serotonin receptor 5-HT_6 (5-HT_6R) attracts special attention due to the significant procognitive activity of its ligands, either agonists or antagonists, confirmed in many preclinical studies [2, 18–21]. However, all the selective 5-HT_6R agents investigated so far have not passed clinical trials, mainly due to the insufficient activity in patients compared to that observed in animal models [2].

Taking into account the complex aetiology of AD, the additional action of 5-HT_6R ligands on either CDK5 or MAO-B would allow finding an innovative drug, with a strengthened therapeutic effect. Therefore, the discovery of multi-targeted agents that combine the activity towards 5-HT_6R with the above-mentioned enzymes seems to be promising way in the search for new AD drugs fitting into the current trend of polypharmacology [22]. In our previous studies, we characterized the highly potent, selective 5-HT_6R antagonists among derivatives of 1,3,5-triazine with confirmed procognitive activity *in vivo* (*e.g.* **1**, Fig. 1). The studies allowed to explore new chemical space thanks to significant structural differences of triazine-based compounds from the previously reported indole-like and/or sulfone-containing 5-HT_6R ligands [23–27]. It can be noticed that triazine-based 5-HT_6R agents characterize a similar structural topology as the reference strong CDK5 inhibitor (**2**), crystallized with CDK5/p25 complex - PDB ID: 3O0G (**1** vs **2**, Fig. 1), which could lead to analogous fitting of these compounds in the binding pocket of the enzyme. Other lines of evidence showed a potency of various triazine derivatives to inhibit CDK5 (**3-5**, Fig. 1) [28–32]. Moreover, several inhibitors of MAO-A and/or MAO-B that contain the 1,3,5-triazine motifs in the structure have been described [7,33,34]. The aforementioned results highlight the potential of triazine derivatives in application for multitargeted AD therapy. This guiding principle resulted in the performing of molecular modelling of our compounds library with particular attention to the possibility of binding to CDK5. Performed *in silico* study confirmed the relevance of the structures designed for synthesis towards inhibition of CDK5 kinase. A series of 25 innovative chemical compounds that combine in their structure the features characteristic for 5-HT_6R ligands and moieties providing interaction with a hinge region pivotal in kinase molecular biology [35,36] have been developed. According to the literature, in order to gain interactions with kinase proteins, the molecule should contain characteristic structural fragments which consist of H-bond acceptor (HBA) and H-bond donor (HBD) being in close distance from each other and sterically available as observed in the already reported CDK5 inhibitors [37].

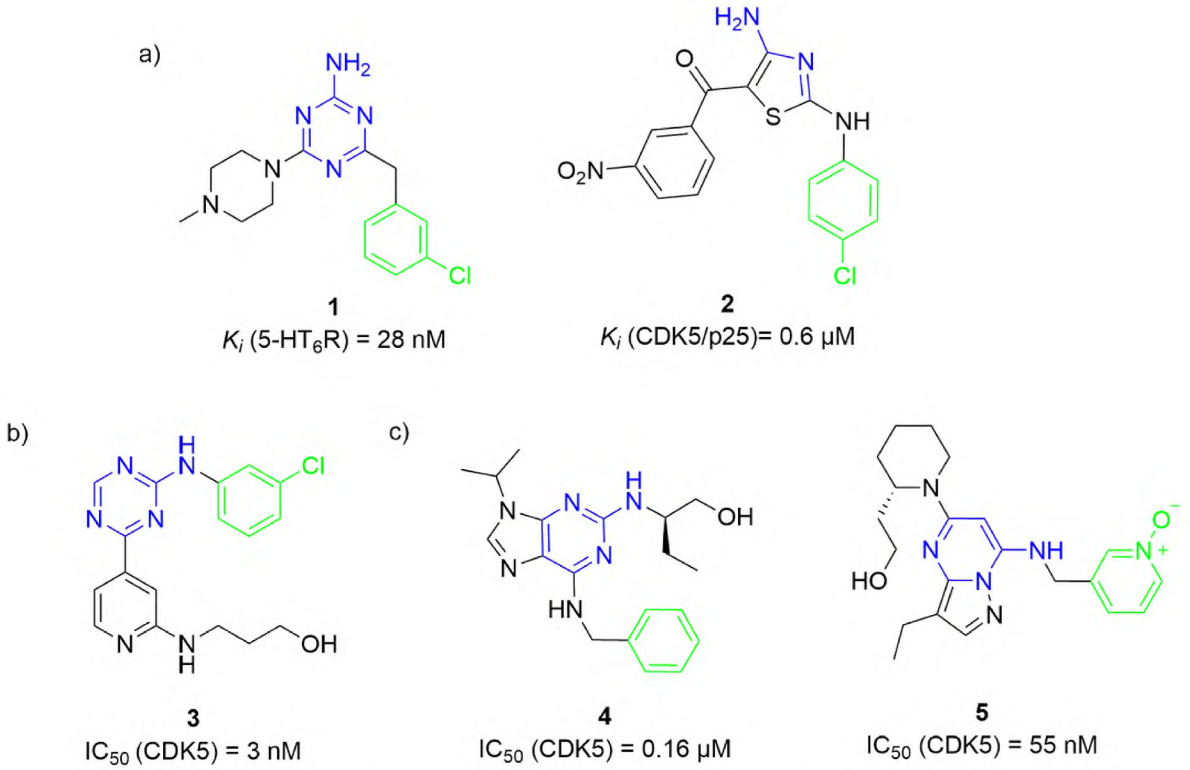

Fig. 1. Structures of triazine 5-HT_6R and CDK5-agents with corresponding motifs marked in colors (blue – topology of 2-amino-triazine-like moiety and green – hydrophobic aromatic); a) structural similarities of representative triazine-based 5-HT_6R antagonist (**1**) [23] and the reference inhibitor crystallized with CDK5/p25 (**2**) [38]; b) CDK5 active agent with 1,3,5-triazine scaffold (**3**) [28]; c) other CDK5 inhibitors: **4** [39] and **5** [10] with structural similarities to **1**.

Such located functional groups form double hydrogen bonds with characteristic hinge region (mainly with Cys83) in the binding pocket of CDK5. This phenomenon has been already confirmed not only by computational prediction but also by X-ray crystallography studies [38].

In our recent research, the phenoxy-derivatives of 1,3,5-triazine with chlorine substituent(s) at the phenyl ring appeared to be especially interesting due to possible halogen-bonding that improved the affinity to the 5-HT_6R [26]. Among them, the 2,5-dichlorophenoxy derivative **6** (Fig. 2) as the highly active agent (K_i = 6 nM) with the potent 5-HT_6R antagonistic action in the functional bioassay (K_B = 27 pM) and selectivity with respect to other GPCRs' off-targets, *i.e.* 5-HT_{1A}, 5-HT_{2A}, 5-HT_7 and D_2 dopamine receptors, was found. Compound **6** also exhibited significant procognitive effects *in vivo* in the Novel Object Recognition (NOR) test in rats, but its active dose was higher than that of other triazine compounds with even weaker affinities for 5-HT_6R [27,40]. An insight into the drug-like profile indicated that this compound (**6**) had rather poor metabolic stability, while the precipitation (poor solubility) during the hepatotoxicity assay *in vitro* made it impossible to determine its exact safety [26]. Compound **6** seemed to be a good starting point for further pharmacomodulation and therefore it was chosen as a lead structure for the present studies.

The previous results for the triazine 5-HT_6R agents have proved that even small changes in position and number of chlorine substituents at the phenyl ring caused significant differences in both, *in vitro* and *in vivo* biological profiles of the compounds [26,27,41]. However, a question of the chlorine atom replacement with different substituents, especially with another halogen, was not explained to date. Thus, in the present study, we aimed to examine the role of the exchange of chlorine into fluorine or fluorine-containing substituents for the considered pharmacological profile, including the inhibition of enzyme targets (MAO-B, CDK5) desirable in search for new complex therapy of AD. Fluorine has been selected as the major component of the modifications at 4-position of 1,3,5-triazine ring as its presence might bring many benefits, e.g. lower molecular mass, better metabolic stability, and lower toxicity risk, while still retaining the desirable electron- and hydrophobic properties of introduced substituents [42,43]. As a second modification, the substitution of an amino group (at position 2 in the triazine ring) with an additional aromatic ring (phenyl or 4-pyridine) was also considered noteworthy for increasing the lipophilicity of the compound (Fig. 2).

The fixed 2,5-substitution topology of the phenyl ring and the ethyl linker branching were of our main interest. For comparison, the 2,3-disubstituted topology, which has corresponding electron and hydrophobic properties but different steric ones, was also taken into consideration. Furthermore, the shorter (methyl) linker branching, which enhanced the 5-HT_6R activity for some triazine-compounds described earlier [26], was taken into account. In this context, a series of twenty-five new triazine derivatives (**7-31**) as chemical modifications of the lead **6** was rationally designed (Fig. 2). In this paper, molecular modelling, synthesis, radioligand binding assays towards the 5-HT_6R and off-targets for the investigated series were presented. An analysis of the 3D-structure for one representative, with the use of experimental X-ray crystallographic analysis, was performed. For selected active compounds, extended biological screening, *i.e.*: functional assays, inhibiting properties for enzymes (CDK5, MAO-B) and "drug-likeness" screening *in vitro*, with special attention to the influence on platelet aggregation, as well as *in vivo* behavioral studies on procognitive, antidepressant- and anxiolytic-like effects, were performed. At the end, structure-activity relationship (SAR) analysis based on obtained results was discussed.

2. Results

2.1. Computer-aided design in search for additional action on CDK5

In order to check out a potency to modulate the activity of CDK5 for the 1,3,5-triazine-piperazine compounds explored by us, and consequently, to rationally design pertinent chemical modifications that could improve the action, molecular modelling study was used. In the first step, compounds **7-25** were docked to the CDK5 crystal structure (**2**, PDB ID: 3O0G). Two CDK5 ligands present in the CHEMBL database with the triazine core were selected as reference structures (Fig. 3).

Both, the series **7-25** and the reference pair (CHEMBL1980246 and CHEMBL1986666) were well docked to the CDK5 binding pocket. Example docking poses for compounds **7**, **14**, **22** and **23** are shown in Fig. 4. The comparison of docking poses of the reference compounds and compounds **7-25**, as well as analysis of the CDK5 binding pocket indicated that it might be beneficial to expand the molecule from the triazine side by addition of another aromatic moiety. The reference compounds are quite well aligned with compounds **7-25** in the binding pocket; however, in all cases, one of the aromatic moieties of the reference structures is not covered by the synthesized compounds.

Taking the conclusion from the first step into account, a small series of compounds (**26-31**) with an additional aromatic moiety at the triazine NH substituent were designed. In the next step, the designed compounds (**26-31**) were docked to the CDK5 binding pocket. Selected docking poses (for **26, 27** and **31**) with reference to the structures from the CHEMBL database are presented in Fig. 5.

The docking poses found (Fig. 5) indicate that substitution by additional aromatic moiety extended the ligand-protein contact network of the synthesized compounds; all aromatic moieties of the reference

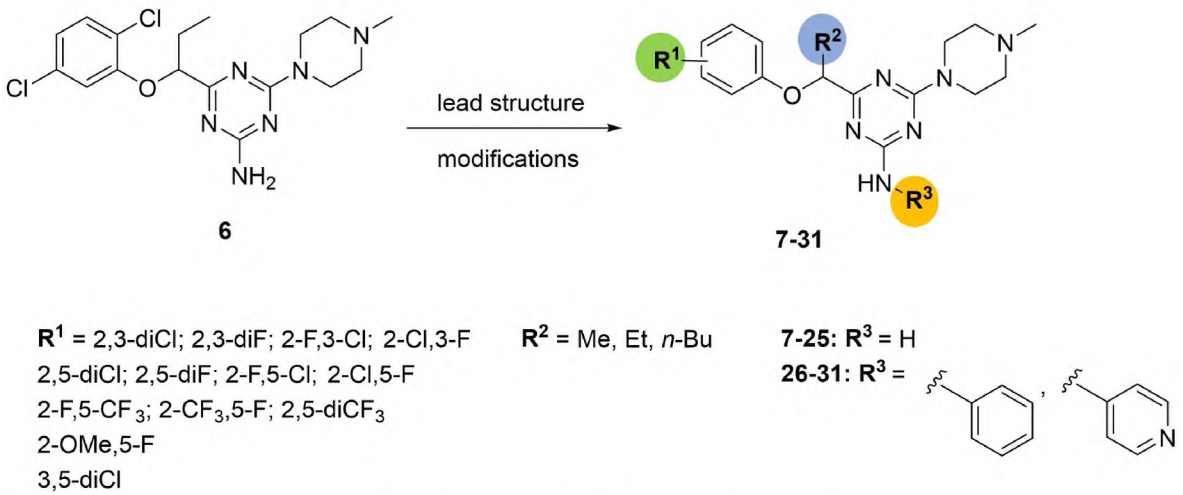

Fig. 2. Lead structure **6** and its arranged modifications.

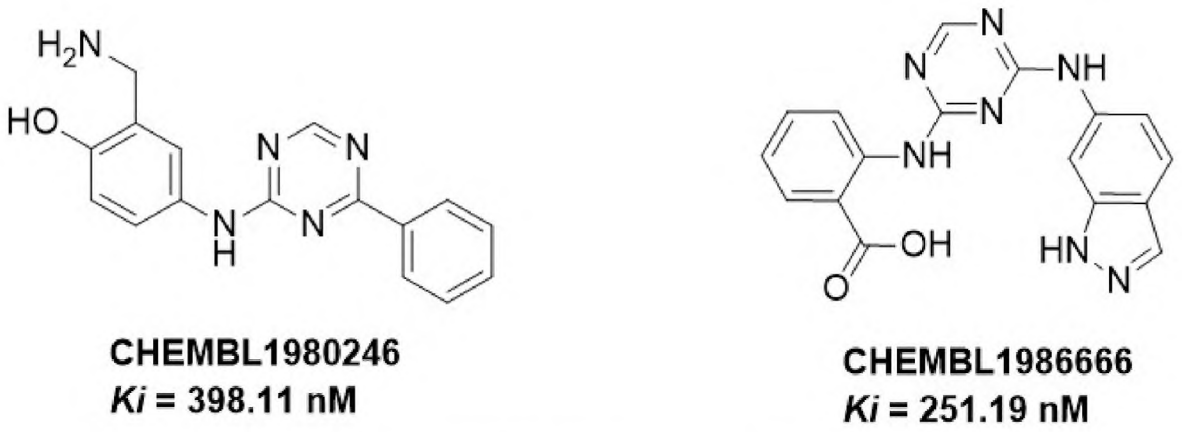

Fig. 3. Reference literature compounds used in the CDK5 modelling studies.

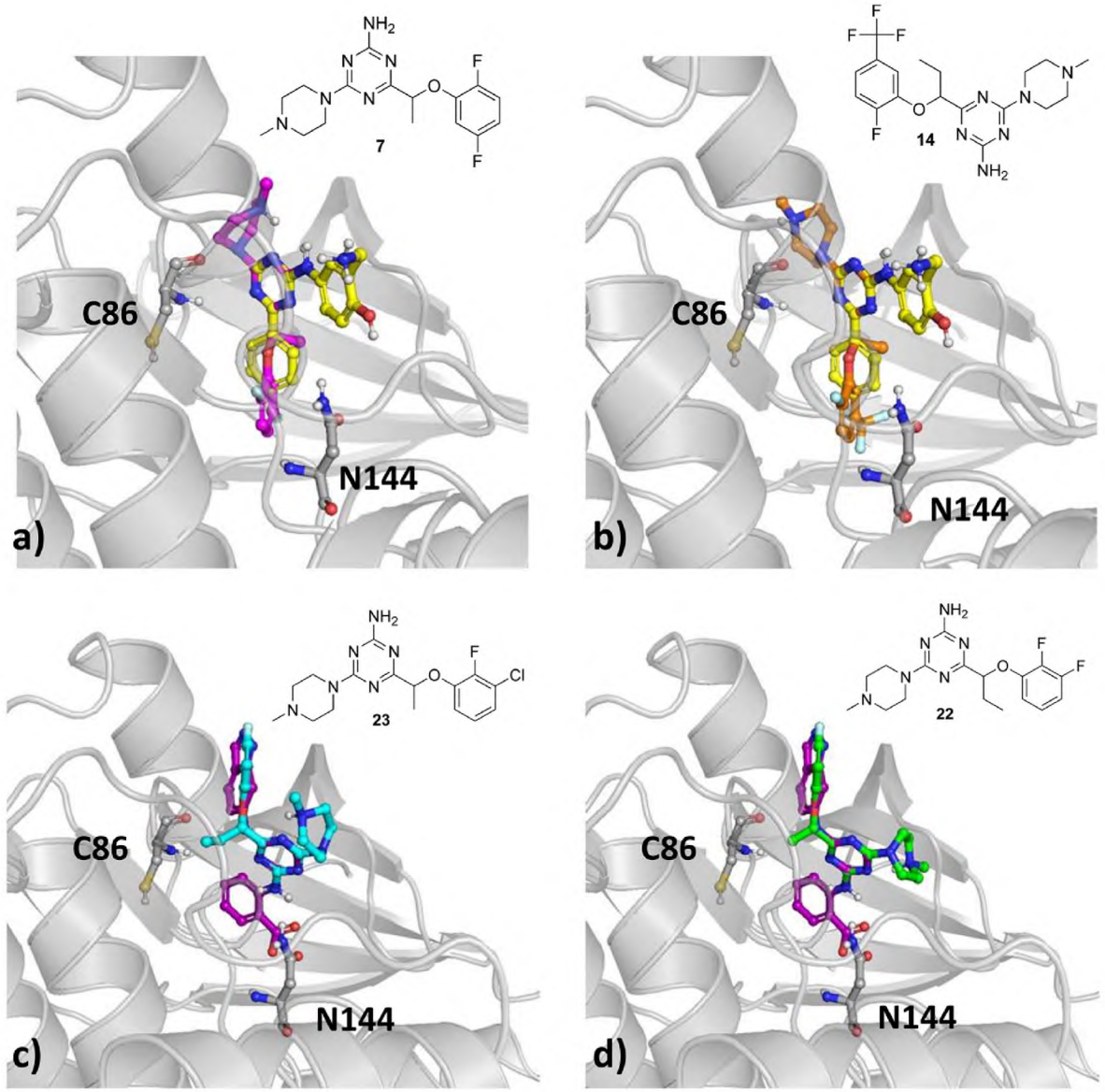

Fig. 4. Docking results to CDK5 for the reference compounds and selected compounds from the group **7-25**: a) CHEMBL1980246 (yellow) and **7** (magenta); b) CHEMBL1980246 and **14** (orange); c) CHEMBL1986666 (purple) and **23** (cyan); d) CHEMBL1986666 and **22** (green).

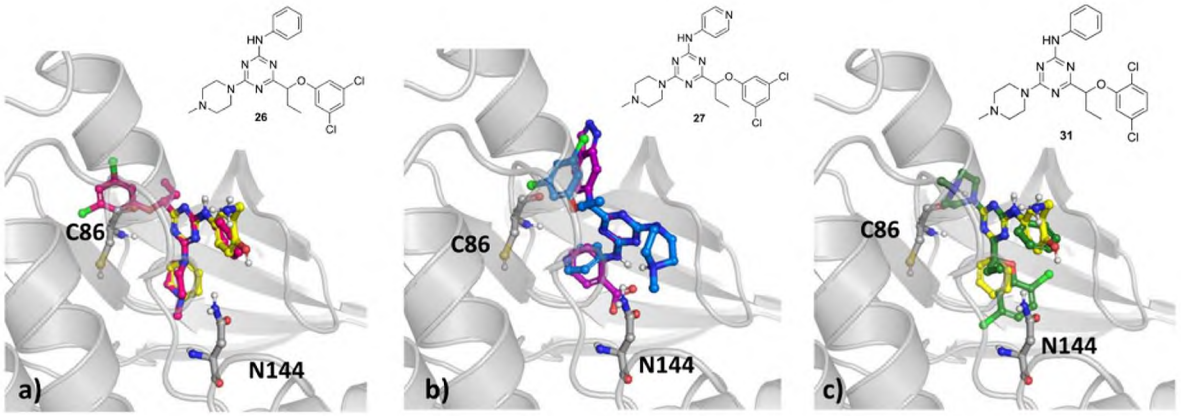

Fig. 5. Docking results to CDK5 for the newly designed compounds: a) **26** (pink), b) **27** (blue), c) **31** (dark green). CHEMBL data shown for reference: CHEMBL1980246 (yellow), CHEMBL1986666 (purple).

compounds are well aligned with the respective parts of the compounds **26-31** (especially for CHEMBL1090246). Results of the molecular modelling simulation confirmed a possibility of the additional inhibitory action towards CDK5 for both sets of triazines (**7-25** and **26-31**) with significantly higher probability for the last series (**26-31**). Thus, it was decided to synthesize the whole series (**7-31**), and perform its pharmacological evaluation *in vitro*, including the CDK5 inhibitory assays for all representatives from the group **26-31**, and for selected ones from the group **7-25**.

2.2. Synthesis

The final compounds (**7-25**) were obtained within the synthetic route (Scheme 1) based on the procedures described previously for the chlorine-derivatives of 1,3,5-triazines [26]. Before the main route, the biguanide intermediate (**32**) was synthesized (Scheme 1a). Then, the compounds **7-25** were obtained in 2-step synthesis pathways (Scheme 1b). The appropriate aromatic ether esters (**33-51**) were formed by nineteen *O*-alkylations of corresponding commercial phenols with, either the methyl 2-bromopropanoate or the methyl 2-bromobutanoate, in the first step (Scheme 1b). The intermediates (**33-51**) reacted with **32** by the cyclic condensation to form final products (**7-25**, Scheme 1b). The aromatic ethers (**33-51**) and consistently final compounds (**7-25**) were obtained as racemic mixtures.

The final compounds (**26-31**) were synthesized in Buchwald-Hartwig reaction (Scheme 2) using the commercial phenyl bromide (**55**) or 4-bromopyridine (**56**) and the appropriate final dichlorophenoxy-1,3,5-triazine derivative (**6, 52-54**) obtained previously [26]. Additional chemical data are provided in Supplementary Material.

2.3. Crystallographic analysis for 22

For the series of 1,3,5-triazines (**7-31**), intensive attempts were made to obtain a crystal suitable for X-ray analysis, which was successful in the case of one representative, i.e. **22**. 3D structure for compound **22** was investigated and compared with that of lead **6** [26], by the use of X-ray

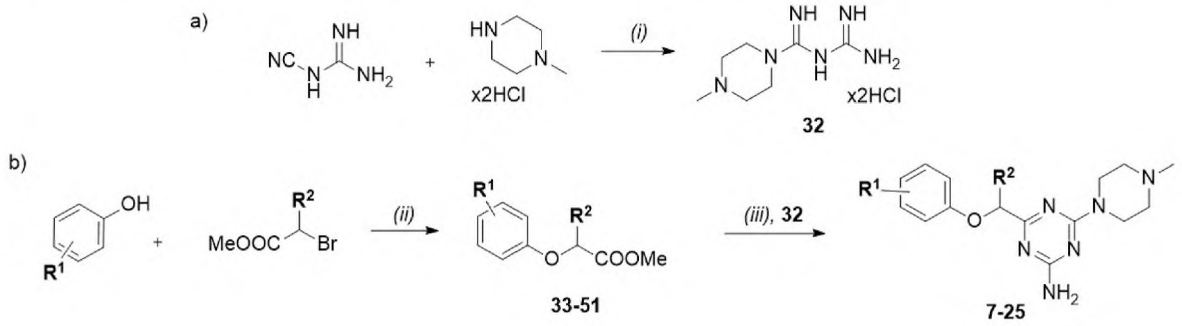

7, 33: R^1 = 2,5-diF, R^2 = Me;
8, 34: R^1 = 2,5-diF, R^2 = Et;
9, 35: R^1 = 2-F,5-Cl, R^2 = Me;
10, 36: R^1 = 2-F,5-Cl, R^2 = Et;
11, 37: R^1 = 2-Cl,5-F, R^2 = Me;
12, 38: R^1 = 2-Cl,5-F, R^2 = Et;
13, 39: R^1 = 2-F,5-CF_3, R^2 = Me;
14, 40: R^1 = 2-F,5-CF_3, R^2 = Et;
15, 42: R^1 = 2-CF_3,5-F, R^2 = Me;
16, 42: R^1 = 2-CF_3,5-F, R^2 = Et;
17, 43: R^1 = 2,5-diCF_3, R^2 = Me;
18, 44: R^1 = 2,5-diCF_3, R^2 = Et;
19, 45: R^1 = 2-OMe,5-F, R^2 = Me;
20, 46: R^1 = 2-OMe,5-F, R^2 = Et;
21, 47: R^1 = 2,3-diF, R^2 = Me;
22, 48: R^1 = 2,3-diF, R^2 = Et;
23, 49: R^1 = 2-F,3-Cl, R^2 = Me;
24, 50: R^1 = 2-F,3-Cl, R^2 = Et;
25, 51: R^1 = 2-Cl,3-F, R^2 = Et;

Scheme 1. Synthetic route for compounds **7-25**. Reagents and conditions: *(i)* BuOH, reflux, 16h, yield: 86%; *(ii)* acetonitrile, K_2CO_3, reflux, 1–16 h, yield: 36–98%; *(iii)* absolute methanol, Na, reflux 16 h, yield: 21–58%.

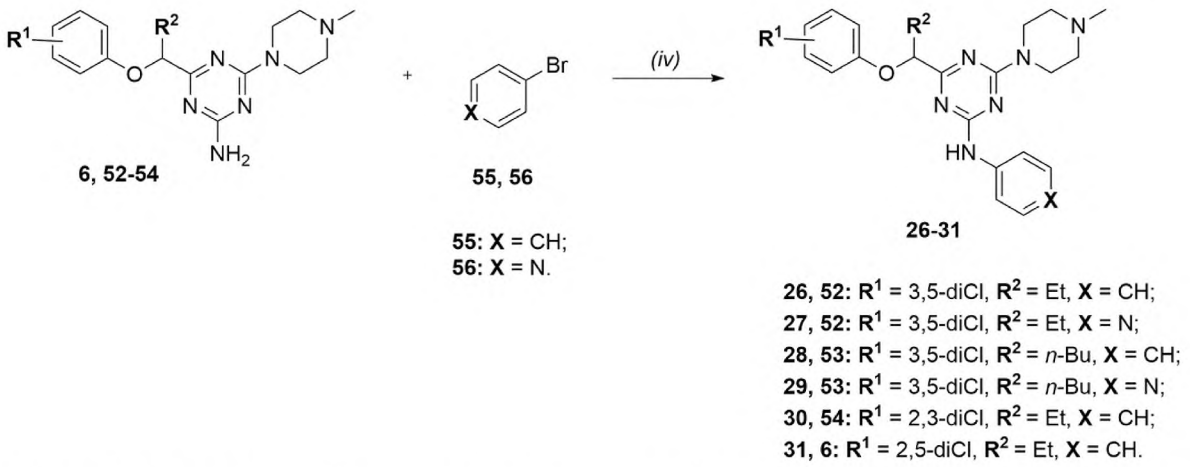

Scheme 2. Buchwald-Hartwig reaction for compounds **26-31**. Reagents and conditions: *(iv)* sodium *tert*-butoxide, RuPhos Pd G3, 1,4-dioxane, 100 °C, 3h, yield: 27–41%.

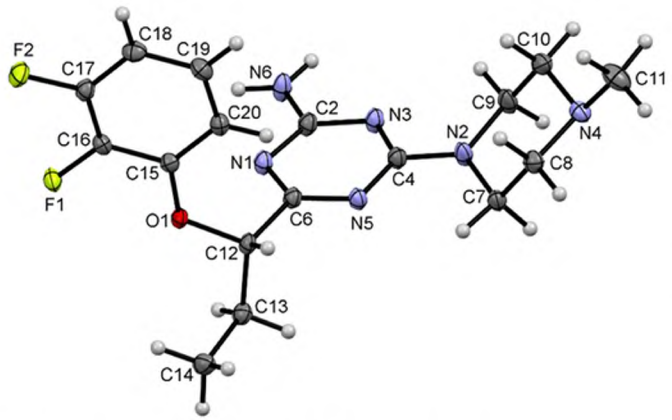

Fig. 6. The molecular geometry of **22** with the atom numbering schemes. Displacement ellipsoids are drawn at the 50% probability level.

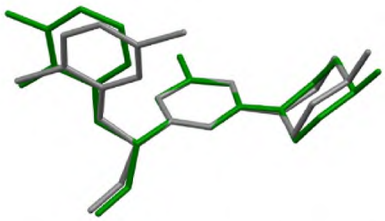

Fig. 7. The overlap of the triazine rings of **22** (green) in the crystal and lead **6** containing 2,5-dichloro substituents at aromatic ring (grey) in a crystal structure published previously [26]. Hydrogen atoms have been omitted for clarity.

analysis. The projection of molecular geometry in the crystal of **22** is presented in Fig. 6.

The triazine ring is almost planar with an r.m.s. deviation from planarity of fitted atoms (N1, C2, N3, C4, N5 and C6) of 0.0065 Å. The nitrogen atoms at C2 and C4 atoms are coplanar with triazine ring (deviation from this plane 0.0018 Å). An analysis of the bond lengths C-N for both nitrogen atoms (N2 and N6) shows the values of 1.35 and 1.34 Å, indicating conjugation of these atoms with the triazine ring. The piperazine ring adopts chair conformation with equatorial position of the methyl group at the N4 atom and intermediate location of the substituent at N2 atom between equatorial and axial position, as indicated by the torsion angle C4-N2-C9-C10 being 124.7(1)° (for equatorial position value about 180° and for axial 60°). This value is similar to values observed in other triazine derivatives, for which we determined crystal structures earlier [26]. The interplanar angle between triazine and piperazine rings is 53.52(5)°, while between triazine and aromatic ring is 87.02(4)°. The geometry of this compound (**22**) is similar to that of lead (**6**) containing 2,5-dichloro substituents (Fig. 7) [26].

The main motif of intermolecular interactions is based on N-H···N hydrogen bonds (Fig. 8), leading to the formation of C(9) chains in the crystal lattice. This type of interactions was not observed in the more active compound **6**. The second hydrogen atom at the N6 atom is also engaged in the hydrogen bond with the N3 atom of another molecule related by the inversion center. These interactions lead to the formation of dimers, also observed in the crystal structures of lead compound **6** and another derivative published earlier [26]. Furthermore, the crystal structure is stabilized by C-H···N, C-H···O and C-H···F contacts. Parameters of these interactions are presented in Table 1. Thus, for the less active compound **22** N-H···N hydrogen bonds with engagement of nitrogen atom of piperazine ring as acceptor and C-H···O hydrogen bonds are observed, which are not present in the crystal structure of more active compound **6**.

2.4. Pharmacology

2.4.1. GPCR binding profile

2.4.1.1. Radioligand binding assay. All newly synthesized compounds (**7-31**) have been assessed on their affinities for GPCR receptors, including the 5-HT_6R main target and the off-targets (serotonin 5-HT_{1A}R, 5-HT_{2A}R, 5-HT_7R and dopaminergic D_2R), in the radioligand binding assay (RBA). The whole series (**7-31**) showed potent affinities (K_i < 100 nM) for the 5-HT_6R and significant selectivity over the off-targets (Table 2, Table S1 in the Supplementary Material). In particular, nine compounds (**8, 10, 12, 14, 16, 25, 26, 30, 31**) displayed very strong affinity (5-HT_6R: K_i < 20 nM) and significant selectivity over other GPCRs (20–600 fold). Compound **8** turned out to be the most potent 5-HT_6R agent, which exhibited even stronger binding (K_i = 5 nM) than that of lead (**6**).

2.4.1.2. Molecular modelling for the interactions with 5-HT_6R. An induced fit docking approach was used to dock the newly synthesized derivatives (**7-31**) to the crystal structure of the 5-HT_6R (PDB ID: 7XTB). Results for compound **22** indicated the high geometry alignment of the modelled conformation with that coming from the crystallographic analysis (see Supplementary, Fig. S6). It should be noted, that results of the molecular modelling showed a high consistency with the binding mode reported previously for 1,3,5-triazine derivatives using our 5-

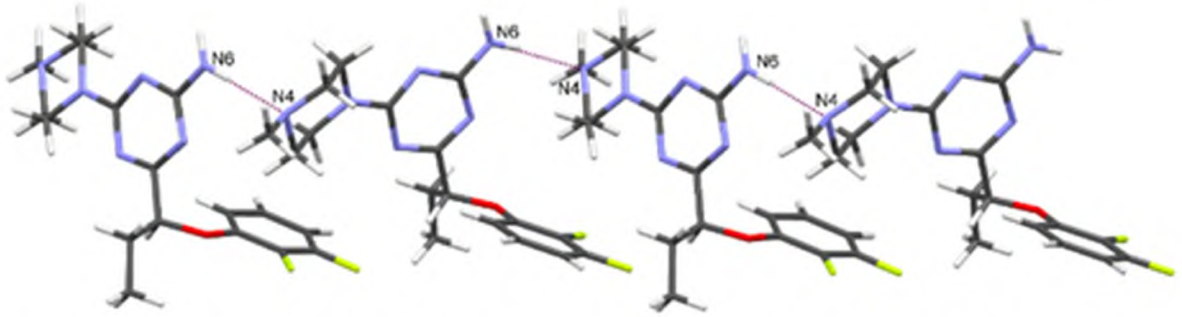

Fig. 8. Partial packing view of **22**, illustrating the creation of chain in [001] direction. Dashed purple lines indicate hydrogen bonds.

Table 1
Parameters of intermolecular interactions in the crystal of **22**.

D-H···A	H···A (Å)	D···A (Å)	D-H-A (°)	Symmetry code
N6-H6B··· N3	2.23	3.121(1)	171.8	-x+1, y, -z+1/2
N6-H6A···N4	2.18	3.049(1)	170.5	-x+1, y, -z+1/2
C8-H8B···N1	2.69	3.358(2)	125.4	x, -y+1, z+1/2
C12-H12···F2	2.60	3.540(1)	156.2	x, -y+1, z-1/2
C18-H18···F1	2.57	3.255(1)	129.4	x, -y+1, z-1/2
C19-H19···O1	2.62	3.552(1)	168.5	x, y+1, z

HT_6R homology models [21,23,24,26]. On this basis, the effect of fluorine substitution on the interaction in the binding pocket was also compared.

Analysis of the binding mode (Fig. 9a) indicated the salt bridge between positively charged nitrogen (from *N*-methylpiperazine ring) and the negatively charged side chain of aspartic acid D3.32, the CH–π/π–π interactions with phenylalanine F6.51 and/or F7.34, and hydrogen bond between the primary amino group of 1,3,5-triazine core and the carbonyl oxygen of alanine A5.42. The substituted aromatic moiety linked with the 1,3,5-triazine ring was exposed to the hydrophobic cavity constituted by transmembrane helices TM3–TM5 and extracellular loop 2 (ECL2). Comparison of the binding modes of F-, Cl-, and CF_3-substituted in positions 2- and 5- derivatives showed coherent orientations of this moiety in the hydrophobic cavity, stabilized additionally by the CH-π interaction with H167. The 2,5-diCl derivative **6** was found to form halogen bonds (all with backbone carbonyl oxygen) with alanine A4.56 (XB distance = 3.2 Å, σ-hole angle = 165°) formed by chlorine in position 5. The fluorinated analogues **8** and **18** formed the dipole-dipole stabilization interaction with C═O bonds of alanine A4.56 and a partially the side chain of S4.57. An extension of the 1,3,5-tritriazine derivatives by adding at position 2 an additional aromatic ring showed retaining the high activity towards 5-HT_6R. Molecular docking revealed that this can be related to the formation of stabilizing CH-π/π-π interactions between the additional aromatic ring of compound **31** and residues W6.48 and F5.47 (Fig. 9b).

2.4.1.3. Structure – 5HT$_6$R affinity relationship. All the newly synthesized compounds (**7-31**) showed high affinities for 5-HT_6R with K_i values lower than 100 nM, and nine of them displayed a very strong affinity towards 5-HT_6R (K_i < 20 nM). The results obtained in this work allow for a discussion on structure-activity relationships, taking into account the role of the substitution at the phenyl ring with respect to the length of linker branching and the meaning of an additional aromatic moiety at the triazine NH_2 group.

As the length of the linker branching (methyl *vs* ethyl) is concerned, the ethyl branching was distinctly more favorable for the 5-HT_6R affinity than the methyl one. It can be confirmed along with the whole series, with exception of two members containing methoxy group at the phenyl ring (**19**, **20**, Table 2). A similar trend was also observed for the dichloro-substituted series [26]. In the case of ethyl branched compounds (**6**, **8**, **10**, **12**, **14**, **16**, **18**, **20**, **22**, **24** and **25**) the affinity for 5-HT_6R was decreasing in the following order: 2,5-diF >2,5-diCl>2-F,5-Cl>2-F, 5-CF_3> 2-CF_3,5-F ~ 2-Cl,3-F> 2-Cl,5-F > 2-F,3-Cl> 2,5-diCF_3 > 2,3-diF > 2-MeO,5-F, while in the case of the methyl-branched compounds (**7**, **9**, **11**, **13**, **15**, **17**, **19**, **21** and **23**) the corresponding order is as follows: 2-CF_3,5-F> 2-F,3-Cl ~2,5-diCF_3 ~ 2-Cl,5-F> 2-F.5-CF_3> 2,5-diF > 2-F, 5-Cl > 2-OMe,5-F> 2,3-diF (Table 2). Although the differences in K_i values are subtle, they allow to notice some trends typical for this series.

First, it can be observed a significant decrease in the 5-HT_6R affinities with the transfer of the fluorine substituents from 5 into the 3-position of the phenyl ring. This is intriguing and divergent from the previous results found for the dichloro-substituted series, where the 2,5-dichlorophenyl compound (lead **6**) and its 2,3-dichloro-analogue demonstrated equal and very potent affinities for the 5-HT_6R [26]. The crystallographic analysis for diCl- (**6**) and diF- (**22**) derivatives may support to explain this issue. In general, the comparison of geometries of the highly active compound **6** and the less active **22** does not show significant differences but a deeper insight shows a decreasing pyramidality of the N2 atom in piperazine ring for **22** in comparison to **6**. The flatter geometry around the N2 atom makes more rigid molecule **22**, which more limits its fit into the receptor-binding pocket. Furthermore, a fluorine atom is more electronegative than chlorine atom, thus strongly influencing the electron distribution within the molecule. The difference seems to be particularly distinct in the case of vicinal 2,3-diF vs. 2,3-diCl substituents, followed by an appropriate decrease in ability of a molecule to form non-covalent interactions.

As another trend, the replacement of the halogen substituent at the phenyl ring with the methoxy one (**19**, **20**) can confirm the unprofitable role of the less hydrophobic and electron-donating substituent for the 5-HT_6R affinity, which was postulated in another previous research [23].

Furthermore, the second modification (the additional aromatic ring) saved the trends of SAR for the linker and the aromatic ring substitution observed in the previous series (**6-25**, **52-54** [32]). Thus, the relatively highest 5-HT_6R affinity was observed for the ethyl linker if compared to the *n*-butyl one (**26** vs. **28**, and **27** vs. **29**). Then, the favorable position in the phenoxyl ring was the 2,3- and 2,5-dichloro substitution compared to the 3,5-position.

2.4.1.4. Functional assays. Selected active compounds with the ethyl linker and structurally differentiated containing various chemical groups at the phenyl ring in position 2,3 (**25** and **30**), 2,5 (**8**, **10**, **12**, **16**, **18** and **31**) and 3,5 (**26**) were subjected to functional assays to investigate their intrinsic activity towards the 5-HT_6R. Compound **18** was chosen because it has two large strong electron-withdrawing CF_3 groups that might possess a significant effect on fitting into the binding pocket. During the experiments, cAMP levels were measured (Table 3). None of the tested derivatives showed agonistic mechanism, while all of them displayed strong antagonistic activity (pK_b = 6.57–8.48) in the low nanomolar range (see details in Table S2, Supplementary Material). Furthermore, the antagonistic potency was in good accordance with their affinities found in the RBA, *i.e.* pK_b was in the similar range in the

Table 2
The results from radioligand binding assays for the investigated compounds **7-31**.

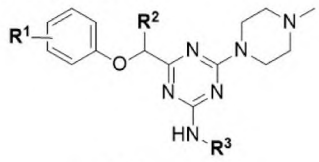

7-31

Compound	R^1	R^2	R^3	K_i [nM]*				
				5-HT_6R	5-HT_{1A}R	5-HT_{2A}R	5-HT_7R	D_2R
Lead 6	2,5-diCl	Et	H	**6**	4760	484	5706	320
7	2,5-diF	Me	H	**56**	3110	2278	21720	1020
8	2,5-diF	Et	H	**5**	3039	573	11530	1633
9	2-F,5-Cl	Me	H	**58**	2019	625	11900	416
10	2-F,5-Cl	Et	H	**11**	4400	770	15120	817
11	2-Cl,5-F	Me	H	**39**	1544	2674	7237	1444
12	2-Cl,5-F	Et	H	**18**	1746	311	-	602
13	2-F,5-CF_3	Me	H	**52**	6075	1464	17100	931
14	2-F,5-CF_3	Et	H	**12**	8273	1172	18790	1079
15	2-CF_3,5-F	Me	H	**30**	6977	629	29570	408
16	2-CF_3,5-F	Et	H	**15**	2906	281	7330	260
17	2,5-diCF_3	Me	H	**35**	5759	797	20000	811
18	2,5-diCF_3	Et	H	**31**	8501	1538	18120	820
19	2-OMe,5-F	Me	H	**60**	6169	2402	107900	2430
20	2-OMe,5-F	Et	H	**72**	4752	819	44990	1788
21	2,3-diF	Me	H	**94**	4719	704	24040	1352
22	2,3-diF	Et	H	**55**	2652	3031	11480	1305
23	2-F,3-Cl	Me	H	**31**	2129	113	9743	472
24	2-F,3-Cl	Et	H	**23**	2942	209	4338	595
25	2-Cl,3-F	Et	H	**15**	1926	2239	8684	3356
26	3,5-diCl	Et	Ph	**7**	19170	1680	16150	565
27	3,5-diCl	Et	Pyr	**66**	4922	437	12570	723
28	3,5-diCl	*n*-Bu	Ph	**21**	143600	287	33590	2589
29	3,5-diCl	*n*-Bu	Pyr	**94**	5141	694	5141	2079
30	2,3-diCl	Et	Ph	**8**	4584	117	2673	411
31	2,5-diCl	Et	Ph	**6**	5397	338	2590	421
Ref	-	-	-	7[a]	32[b]	21[c]	62[d]	9[a]

*Standard deviations are given in the Supplementary Material (Table S1).
[a] Olanzapine.
[b] buspirone.
[c] aripiprazole.
[d] clozapine; 5-HT_6R affinities in bold; Ph – phenyl group; Pyr – 4-pyridyl group.

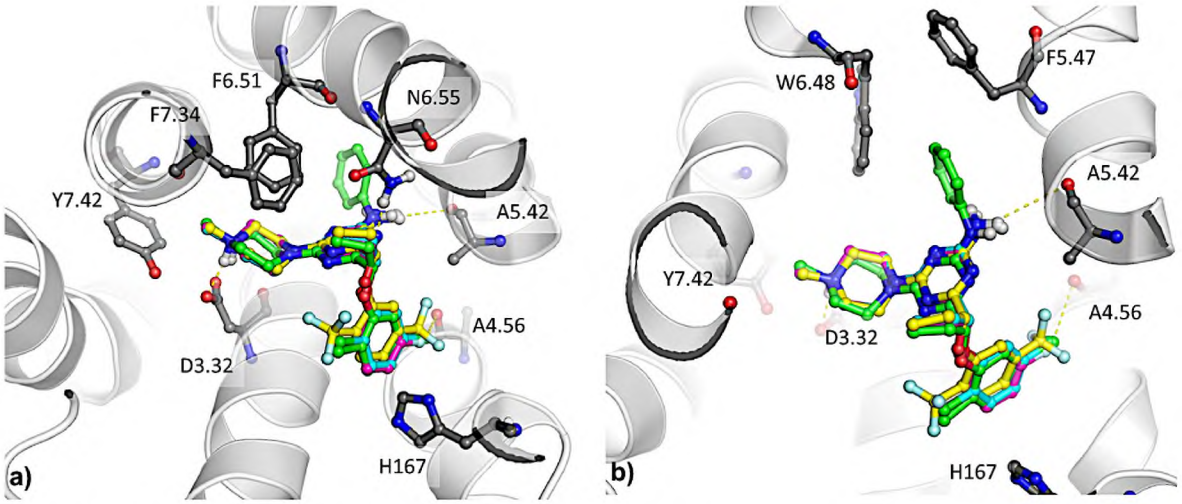

Fig. 9. Illustration of the binding modes of the selected 2,5-disubstituted derivatives within the 5-HT_6R binding site. Binding modes of analogues with chlorine (**6**; cyan), fluorine (**8**; magenta), CF_3 (**18**; yellow), and chlorine but with an aromatic ring connected via NH to triazine (**31**; green). Amino acids that are crucial for the L–R interactions are shown as thick dark-grey sticks.

Table 3
Functional assays results towards 5-HT_6R for representative compounds (**8, 10, 12, 14, 16, 18, 25, 26, 30** and **31**).

Compound	Agonist mode[a] E_{max} [%] ± SEM	Antagonist mode[b] pK_b ± SEM
Serotonin	100.00 ± 2.88	N.T.
Mianserin	N.C.	6.42 ± 0.06
SB258585	N.T.	9.55 ± 0.09
8	10 ± 2.96	8.16 ± 0.02
10	11 ± 4.52	8.23 ± 0.35
12	7 ± 0.35	N.C
14	5 ± 1.44	8.26 ± 0.33
16	8 ± 0.10	N.C.
18	5 ± 3.72	7.69 ± 0.02
25	1 ± 0.58	8.48 ± 0.40
26	9 ± 0.54	6.57 ± 0.05
30	8 ± 0.44	7.13 ± 0.15
31	3 ± N.C.	7.43 ± 0.01

Abbreviations: E_{max} - the maximal response; N.T. – not tested; N.C. - not calculable.

[a] Scores were standardized as a percentage of the maximum agonist response. (Serotonin 10^{-5} M).

[b] Scores were standardized as a percentage of the reference antagonist. (SB258585 10^{-5} M).

case of **8, 10,14** and **25** and slightly weaker for compounds **18, 26, 30** and **31** (Table 2 vs. Table 3).

2.4.2. Enzyme inhibitory profile

2.4.2.1. CDK5 kinase inhibition. In line with the objectives of this study and based on the molecular modelling prediction, selected active and structurally differentiated 5-HT_6R antagonists (**8, 10, 14, 18, 26-31**) were examined on their inhibiting properties towards CDK5 kinase. The preliminary screening of CDK5 inhibition consisted of measuring the percent of the activity of the enzyme under the influence of the tested compounds. For comparison, the reference CDK5 inhibitor, roscovitine, was used. Results are shown in Table 4. Despite the structural similarities of the tested compounds (**8, 10, 14, 18, 26-31**) to the confirmed CDK5 inhibitors (**2-5**; Fig. 1) and promising results of the molecular modelling simulation performed (Figs. 4 and 5), none showed desirable CDK5 inhibiting effects (percent of enzyme activity <50%) at the 10 μM concentration used in the assay.

2.4.2.2. MAO-B inhibition. Additionally, the selected active 5-HT_6R agents (**8, 10, 14, 18**) were also tested on their activity against the human recombinant monoamine oxidase B (MAO-B) in two concentrations (1 μM and 10 μM) using p-tyramine as substrate (200 μM). Results for the tested compounds were compared to the results for the reference MAO-B inhibitors (rasagiline and safinamide at 1 μM). Based on the results obtained, all tested triazine compounds (**8, 10, 14, 18**) displayed insignificant MAO-B inhibiting properties causing lower than 50% inhibition of the enzyme at both tested concentrations (details in Table S3, Supplementary Material).

Table 4
The results from CDK5/p25 inhibition assay. Tested compounds applied at 10 μM concentration.

Compound	Percent of enzyme activity* ± SEM
Roscovitine[a]	14.5 ± 1.19
8	102.5 ± 4.19
10	106.2 ± 5.20
14	93.3 ± 4.05
18	92.0 ± 2.12
26	100 ± 4.97
27	103 ± 2.00
28	105 ± 8.70
29	101 ± 5.70
30	95 ± 6.76
31	106 ± 2.10

*The results were expressed as means from two experiments performed in duplicates.

[a] Roscovitine: IC_{50} = 143.1 nM, pIC_{50} = 6.84 ± 0.24. Dose-response curves for activity of CDK5/p25 were provided in Supplementary Material (Fig. S1).

2.5. ADMET properties

2.5.1. Water solubility

Two of the most active compounds (**8** and **31**) were chosen for the determination of water solubility. Compounds concentration was established using UV spectroscopy in accordance with the method reported previously [44]. Solubility results, presented in Table 5, pointed out that compound **8** is seven times more soluble in water than **31**, which contains additional aromatic ring attached to the triazine.

2.5.2. Permeability

In order to control if the chemical modifications performed allowed to maintain very good membrane permeability of lead **6** [26], the most active compounds with the highest 5-HT_6R affinity and varied 2,5- position substitution (**8, 10** and **14**) were submitted for PAMPA assay. The poor solubility of **31** disqualified this compound from the test. The assay concerns passive penetration through artificial membranes which imitate barriers for compound absorption from the intestines with a good correlation to *in vivo* conditions. It was performed following the previously referred protocol [26,40] and manufacturer's guidelines [45]. Results are shown in Table 6.

All the examined compounds demonstrated an excellent permeability, with *Pe* values higher than that of the high-permeable reference, caffeine (CFN, $Pe = 15.1 \times 10^{-6}$ cm/s), and much higher than the breakpoint for permeable compounds according to manufacturer's guideline ($Pe \geq 1.5 \times 10^{-6}$ cm/s). These results demonstrate that compounds **8, 10** and **14** had even better permeability than that of lead **6**, which may confirm the validity of the modifications performed.

2.5.3. Metabolic stability

The most active representatives of both structural modifications (**8, 10, 14** and **31**) were tested for their metabolic stability. The assay was performed *in vitro* by using rat liver microsomes (RLMs). Results were compared to those of lead (**6**) [26,27], and the unstable reference drug verapamil (Table 7). In the previous studies for **6**, the formation of six metabolites was observed after the incubation with RLMs, and more than 90% of **6** was biotransformed [26]. The main metabolites were formed by demethylation, single or multiple hydroxylation and decomposition of the piperazine ring. In the case of verapamil which was biotransformed in more than 60%, three metabolites were found. Similarly to **6**, compounds **10** and **14** were biotransformed in more than 90%, resulting in the formation of nine metabolites of **10** and six metabolites of **14**. Their found metabolic pathways were alike to **6**. In contrast, compound **8**, the 2,5-difluoro- structural analogue of **6**, displayed the great *in vitro* phase I metabolic stability. Only two metabolites in the range of 5% were observed following the incubation with microsomes, and 95.12% of **8** remained in the reaction mixture. In contrast, compound **31** showed moderate metabolic stability (70.43% of **31** remained in the reaction mixture after incubation with RLMs) and three metabolites have been established.

Predicted *in silico* metabolites are proposed in Table 7, while the proposed sites of metabolism are presented in Fig. 10.

Table 5
Water solubility of compounds **8** and **31**.

Compound	Solubility [mg/ml]	Solubility [mmol/l]
8	0.079	0.2168
31	0.015	0.0317

Table 6
Permeability coefficient of compounds **8**, **10** and **14**.

Compound	*Pe** [10^{-6} cm/s] ± SD
CFN	15.1 ± 0.4
6	18.9 ± 0.9**
8	20.6 ± 2.1
10	30.0 ± 3.5
14	19.0 ± 0.4

CFN – caffeine. *Tested in triplicate. ***Pe* value revealed in previous studies [26,27].

The most common metabolic reaction was demethylation and hydroxylation, which was observed for the lead compound **6**, as well as for **10** and **14** but neither for compound **8** nor **31**. Compounds **6**, **10** and **14** were metabolically unstable even more than the reference verapamil. Mass spectra of the control sample and the test sample are included in the Supplementary Material (Figure S3a-s).

Due to so promising behavior, the compound **8** has been intended for phase II metabolism studies. The assay was performed *in vitro* by using rat liver microsomes (RLMs).

After 1 h, 82,61% of the parent compound remained in the reaction mixture and 12,26% of glucuronidated metabolites M3 and M4 were observed (Supplementary Material, Figs. S4a, b, c). The phase II control reaction with the reference compound 7-hydroxy-4-(trifluoromethyl)

Table 7
The molecular masses and metabolic pathways of compounds **8**, **10**, **14** and **31**.

Substrate	Molecular mass [*m/z*]	% of remaining compound	% of metabolite in the reaction mixture	Retention time [min.]	Molecular mass of the metabolite [*m/z*]	Proposed metabolic pathway[a]
6[b]	397.22	8.93	33.99	3.75	413.24	hydroxylation
			27.04	4.91	413.24	hydroxylation
			11.30	3.67	399.22	demethylation and hydroxylation
			9.13	4.65	383.20	demethylation
			7.17	3.95	429.26	double hydroxylation
			2.43	3.26	429.19	double hydroxylation
8	364.40	95.12	3.48	4.26	381.29	hydroxylation
			1.40	4.30	381.36	
10	381.11	7.86	49.29	5.38	397.21	hydroxylation
			14.86	4.69	399.34	demethylation, double hydroxylation
			9.52	5.09	367.14	demethylation
			5.59	4.48	413.24	double hydroxylation
			5.04	4.18	383.18	demethylation and hydroxylation
			4.09	4.28	397.14	hydroxylation
			1.97	5.62	381.11	demethylation, hydroxylation and dehydrogenation
			0.94	4.90	413.04	double hydroxylation
			0.85	3.51	-	not identified
14	415.24	4.72	51.51	5.73	431.13	hydroxylation
			18.38	5.46	401.20	demethylation
			15.93	4.69	417.30	demethylation and hydroxylation
			4.01	6.14	417.16	demethylation and hydroxylation
			3.75	6.03	433.26	double hydroxylation and ring opening
			1.71	5.08	375.19	fragmentation
31	473.40	70.43	16.74	7.65	489.20	hydroxylation
			6.87	3.43	461.26	decomposition
			5.96	5.67	464.32	decomposition
verapamil[b]	454.60	37.27	33.16	4.94	441.42	demethylation
			15.51	3.99	291.35	decomposition
			14.05	4.67	441.42	demethylation

[a] Estimated according to MS spectra and supported by *in silico* data (see Supplementary Material unit 7).
[b] Results revealed in previous studies: **6** [32], verapamil [46] The same procedure was used for metabolism estimation of triazine derivatives **8**, **10**, **14** and **31**.

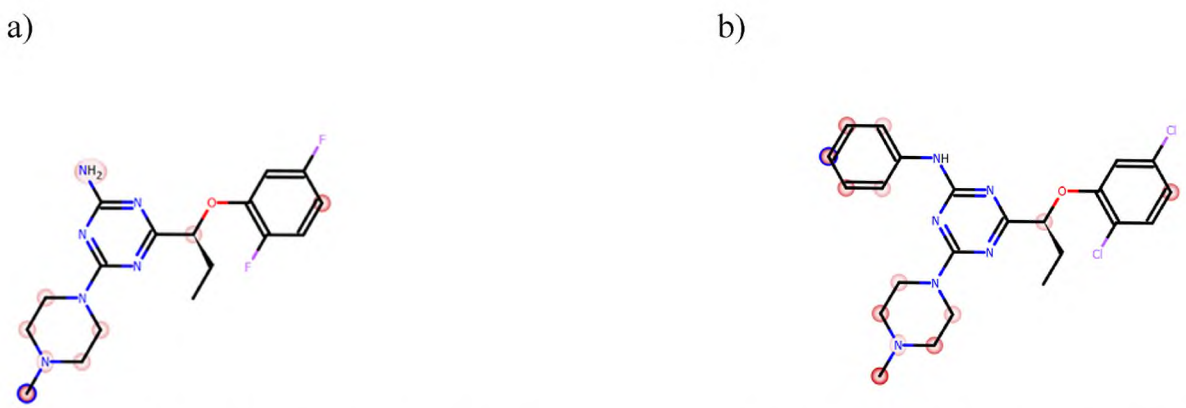

Fig. 10. *In silico* prediction of the sites of metabolism by MetaSite 8.0.1 for a) **8** and b) **31**. Blue circle marked on the functional group structures indicates the highest biotransformation probability. The fading red color shows the decrease of the metabolism probability.

coumarin was also performed (Supplementary Material, Figs. S4d, e, f, g).

In summary, the results from studies on phase I and phase II metabolism of compound **8** confirm its high metabolic stability.

2.5.4. Hepatotoxicity in vitro

The safety profile of three the most active 5-HT_6R agents: **8**, **10** and **14** was assessed in the hepatotoxicity assay *in vitro* using the *hepatoma* HepG2 cell line, following a protocol described previously [26,40,41]. Results were compared to those of reference toxin, doxorubicin, which strongly inhibited the cell viability at 1 μM (DX, Fig. 11).

The tested compounds **8** and **10** showed a statistically significant decrease of cell viability only in the highest concentration (100 μM), while the viability lower than 50% was seen only in the case of **10**. Compound **14**, in a similarity to previously tested lead (**6**), showed a weak hepatotoxic effect also at the concentration of 50 μM [26]. These results indicate very satisfactory *in vitro* safety for the most active 5-HT_6R agent **8**.

2.5.5. Influence on platelet aggregation in vitro

As AD mainly affects the elderly, who often co-suffer from atherosclerotic vascular diseases (*i.e.* coronary artery disease, peripheral atherosclerosis), the drugs used in AD should have also a beneficial effect on the vascular system, e.g. anti-platelet activity, or at least, do not enhance platelet function. As blood platelets express serotonin 5-HT_{2A}R, it is especially reasonable to investigate an influence on platelet aggregation for pharmacologically active compounds with confirmed affinities for 5-HT_{2A}R. Activation of platelets 5-HT_{2A} receptors leads to an increase in intracellular Ca^{2+} level, activation of phospholipase A2 (PLA_2) and arachidonic acid release, amplifying platelets activation [47,48]. In our studies, two of the most active 5-HT_6R agents (**8** and **31**) showed a moderate affinity for the 5-HT_{2A}R (**8**: K_i = 572 nM, **31**: K_i = 338 nM, Table 2), while the weaker affinities for **10**, **14**, **18** (K_i = 0.77–1.54 μM, Table 2) were found. In this context, the compounds (**8**, **10**, **14**, **18** and **31**), investigated in the extended pharmacological assays were also selected to test their influence on platelet aggregation *in vitro*. Rat whole blood was incubated with the tested compounds or vehicle, and the aggregation responses were evaluated with a whole blood aggregometer by measuring the change of impedance. Platelet aggregation was triggered by collagen. Aspirin was used as a reference. Results are shown in Fig. 12.

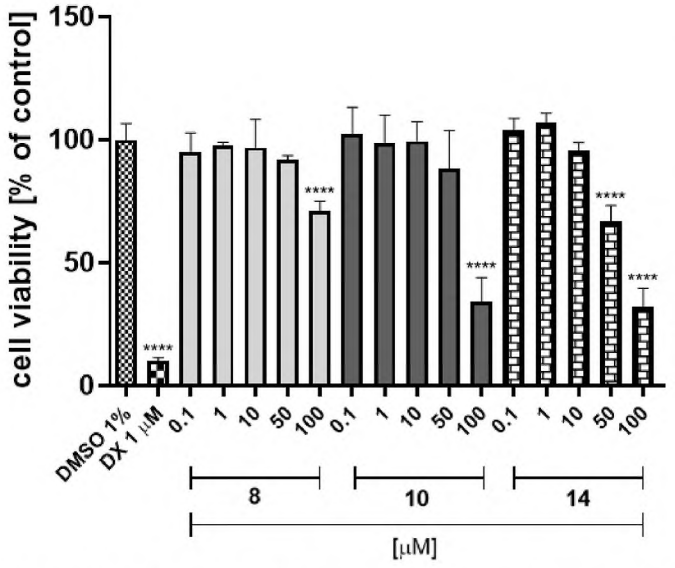

Fig. 11. The hepatotoxicity test of compounds **8**, **10** and **14** with the use of HepG2 cell line. 1 μM of cytostatic drug doxorubicin (DX) was used as positive whereas 1% of DMSO in growth media as a negative control, respectively. GraphPad Prism 8.0.1 was used to calculate the statistical significances by one-way ANOVA, followed by Bonferroni's comparison test (****$p < 0.0001$).

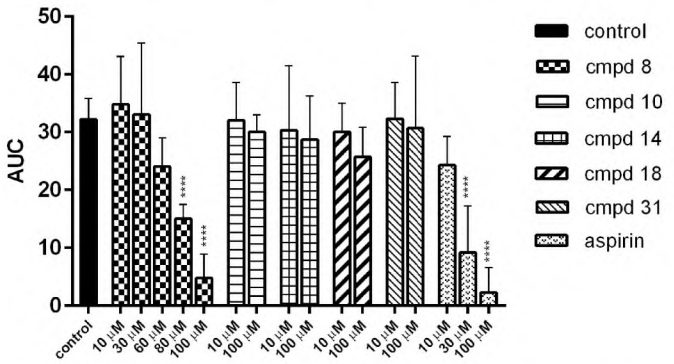

Fig. 12. Effects of the studied compounds **8**, **10**, **14**, **18** and **31** on *in vitro* whole rat blood aggregation induced by collagen (1.6 μg/mL). Results are expressed as mean + Δ/2, where Δ is a width of the 95% confidence interval (CI); n = 3–6; ****$p < 0.0001$ (statistical analysis: one-way ANOVA; post hoc Dunnet test). AUC: area under the curve.

According to the results, compound **8** was able to effectively inhibit collagen-induced aggregation with an IC_{50} value equal to 75.5 ± 2.4 μM. At 100 μM, it decreased platelet aggregation by 85.28%, comparable to aspirin, which inhibited aggregation by 93% at the same concentration, however, the IC_{50} value for aspirin, a COX-1 inhibitor and a standard antiplatelet reference was equal to 18.4 ± 1.6 μM.

In contrast to the compound **8** inhibiting platelet aggregation potently, compounds **10**, **14**, **18** and **31** did not influence platelet aggregation even at the high concentration of 100 μM. Thus, the compounds can be expected safe as they do not interfere with platelet function and probably will possess a negligible risk to cause undesirable effects associated with prolongation of bleeding time.

Summing up, all the tested compounds (**8**, **10**, **14**, **18** and **31**) showed favorable "drug-like" properties in this assay, as none enhanced platelet aggregation *in vitro* in the rat blood. Especially meaningful seems to be the action of compound **8** that decreased platelet aggregation. Hence compound **8**, as the most promising derivative, was chosen for the behavioral studies *in vivo*.

2.6. Behavioral studies in vivo for compound 8

To assess the potential ability of compound **8** to impact cognitive deficits connected with aging or diseases [49], the novel object recognition (NOR) test in rats was performed, allowing to assess episodic memory. Moreover, various previously tested 5-HT_6R antagonists were confirmed effective in that test as well as were able to reverse memory impairments induced by dizocilpine (MK-801), scopolamine or ketamine and other compounds, disturbing memory in rodents [50]. We decided to assess the ability of the potent 5-HT_6R antagonist, compound **8**, to reverse MK-801-induced memory impairment taking into account that this NMDA receptor antagonist induces in rodents memory deficits related to human cognitive disturbances observed in both dementia [51] and schizophrenia [52]. The preference of rats to explore the novel than the familiar object in the T2 session denotes the ability of compound, given jointly with 0.1 mg/kg of MK-801, to reverse MK-801-induced memory impairment in the NOR test. To give thought to rats' preference of novel object exploration, the discrimination index (DI) was used. Its negative value pictures MK-801-induced memory deficit in rats. The selected compound **8**, given at the doses as low as 0.3 and 1 mg/kg, was able to reverse MK-801-induced memory impairments in a statistically significant manner (Fig. 13).

Using the equations proposed by Nair and Jacob (2016) [53] for converting doses between humans and animals based on the body surface area, a minimum active dose of compound **8**, *i.e.* 0.3 mg/kg,

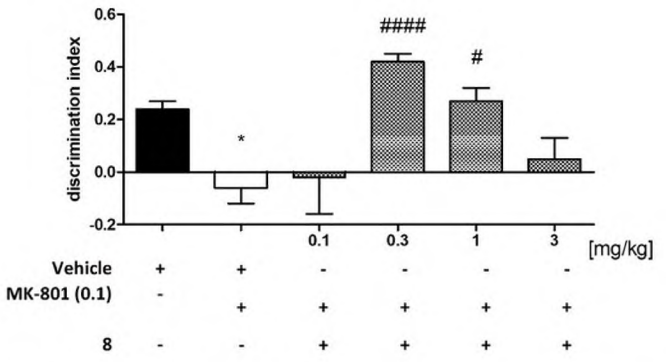

Fig. 13. The ability of compound **8** to reverse MK-801-induced memory disturbances in NOR test. Compound MK-801 was given *i.p.* 30 min while **8** was administered 60 min, before the T1 session. The observation of rats was carried out for 3 min. The data are shown as the mean ± SEM of 6–8 rats, and statistically evaluated by one-way ANOVA followed by Bonferroni's post-hoc test, *p < 0.05 *vs.* vehicle-treated group, while and #p < 0.05, ####p < 0.0001 *vs.* MK-801-treated group, (one-way ANOVA for discrimination index for compound **8** in NOR test: F(5,34) = 8.1709, p < 0.0001).

corresponds to a dose of 3.4 mg in a person weighing 70 kg (standard in Phase I clinical trials).

On the other hand, the compound **8** had no effect on rats' memory when given alone (Fig. 14).

In the next step, the total exploratory time of objects in the recognition phase (T2) was measured after i.p. administration of compound **8** to avoid false-positive results in the NOR test connected with its effect on behavioral parameters. The obtained procognitive results for compound **8**, injected at the dose range 0.1–3 mg/kg alone or jointly with MK-801, in the NOR test seem to be specific, hence the total exploratory time measured during the T2 trial, did not change the total exploratory activity (Table 8).

Among patients with dementia, some neuropsychiatric symptoms such as mood disturbances, anxiety or psychosis are frequently observed. Considering the above, we decided to assess the potential antidepressant- and anxiolytic-like properties of compound **8** using the forced swim test (FST) and elevated plus maze (EPM) test in rats, respectively. Compound **8**, administered at the dose range of 0.3–3 mg/kg, did not show antidepressant-like activity, by decreasing in immobility time, as compared to the control group in the FST (Fig. 15).

In the EPM test, compound **8** given i.p. at the highest investigated dose (3 mg/kg) demonstrated strong anxiolytic-like properties by significantly increasing: the time spent in the open arms (Fig. 16a, by 180%; ANOVA: F(3,25) = 4.9433, p < 0.01), percentage of time spent in

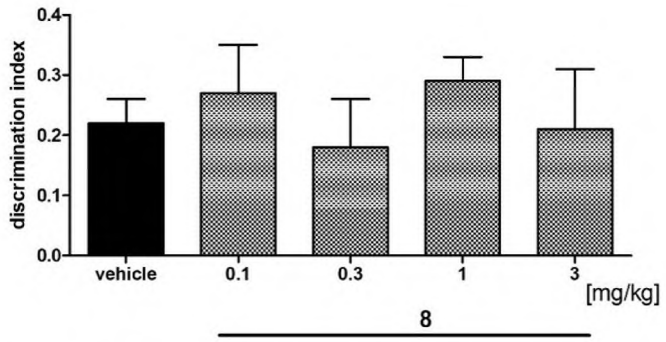

Fig. 14. Effect of compound **8** in rats' NOR test. Compound **8** was administered i.p. 60 min. before the T1 session. The rats were observed for 3 min. The data are presented as the mean ± SEM of 6–8 rats. The data were statistically evaluated by one-way ANOVA followed by Bonferroni's post-hoc test (one-way ANOVA for discrimination index for compound **8** in NOR test: F(4,33) = 0.9593, NS). NS = not significant.

Table 8
The influence of compound **8** on the exploration activity of rats in the NOR test.

Treatment	Dose [mg/kg]	Total exploratory time in T2 session [s]
Vehicle	0	31.86 ± 2.15
8	0.1	38.29 ± 4.13
	0.3	34.63 ± 4.05
	1	39.38 ± 3.73
	3	31.63 ± 2.10
		F(4,33) = 0.9593; NS
vehicle	0 + 0	30.00 ± 2.44
MK-801 + vehicle	0.1 + 0	39.29 ± 3.44
8 + MK-801	0.1 + 0.1	33.25 ± 4.00
	0.3 + 0.1	31.00 ± 5.07
	1 + 0.1	32.57 ± 4.26
	3 + 0.1	27.75 ± 3.81
		F(5,34) = 1.3506; NS

Compound MK-801 was given i.p. 30 min while **8** was administered 60 min, before the T1 session. The observation of rats was carried out for 3 min. Values represent the mean ± SEM of the total exploratory time of both objects during the 3-min test session (T2) compared to the respective vehicle group (one-way ANOVA followed by Bonferroni's post-hoc test); NS = non-significant. N = 6–7.

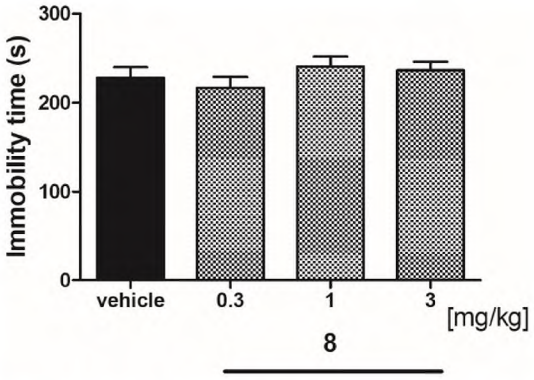

Fig. 15. Effect of compound **8** in rats' FST. Compound **8** was administered i.p. 60 min. before the FST. The rats were observed for 5 min. The data are presented as the mean ± SEM of 6–8 rats. The data were statistically evaluated by one-way ANOVA followed by Bonferroni's post-hoc test (one-way ANOVA for immobility time for compound **8** in FST: F(3,26) = 0.8823, NS). NS = not significant.

the open arms (Fig. 16b, by 188%; ANOVA: F(3,25) = 4.9699, p < 0.01), the number of open arm entries (Fig. 16c, by 140%; ANOVA: F(3,25) = 4.0364, p < 0.05) and the percentage of entries into open arms (Fig. 16d, by 130%; ANOVA: F(3,25) = 4.3375, p < 0.05). Distance travelled in the open arms was also increased; however, the results did not reach a significant level (Fig. 16e, ANOVA: F(3,25) = 1.4842, NS). The lower doses of compound **8** (0.3 and 1 mg/kg) did not cause anxiolytic-like activity in the EPM test (Fig. 16a–e) and had no significant effects on the locomotion (Table S1, Supplementary Material). Hence, the anxiolytic-like activity of compound **8**, measured after its dose of 3 mg/kg in the EPM test (Fig. 16a–e), is likely to reflect a specificity of an action that cannot be explained by competing behaviors.

3. Discussion

Chemical modifications of lead structure **6** were carried out in order to improve both pharmacological profile and ADMET properties of the lead in the search for new drugs useful in the therapy of AD. Multi-targeted action, in which 5-HT_6R would have been the first player possibly strengthened by inhibition of CDK5 (or MAO-B), was supposed to be an additional value. The rationally planned modifications consisted of the replacement of one or two chlorine atoms of the lead **6** with

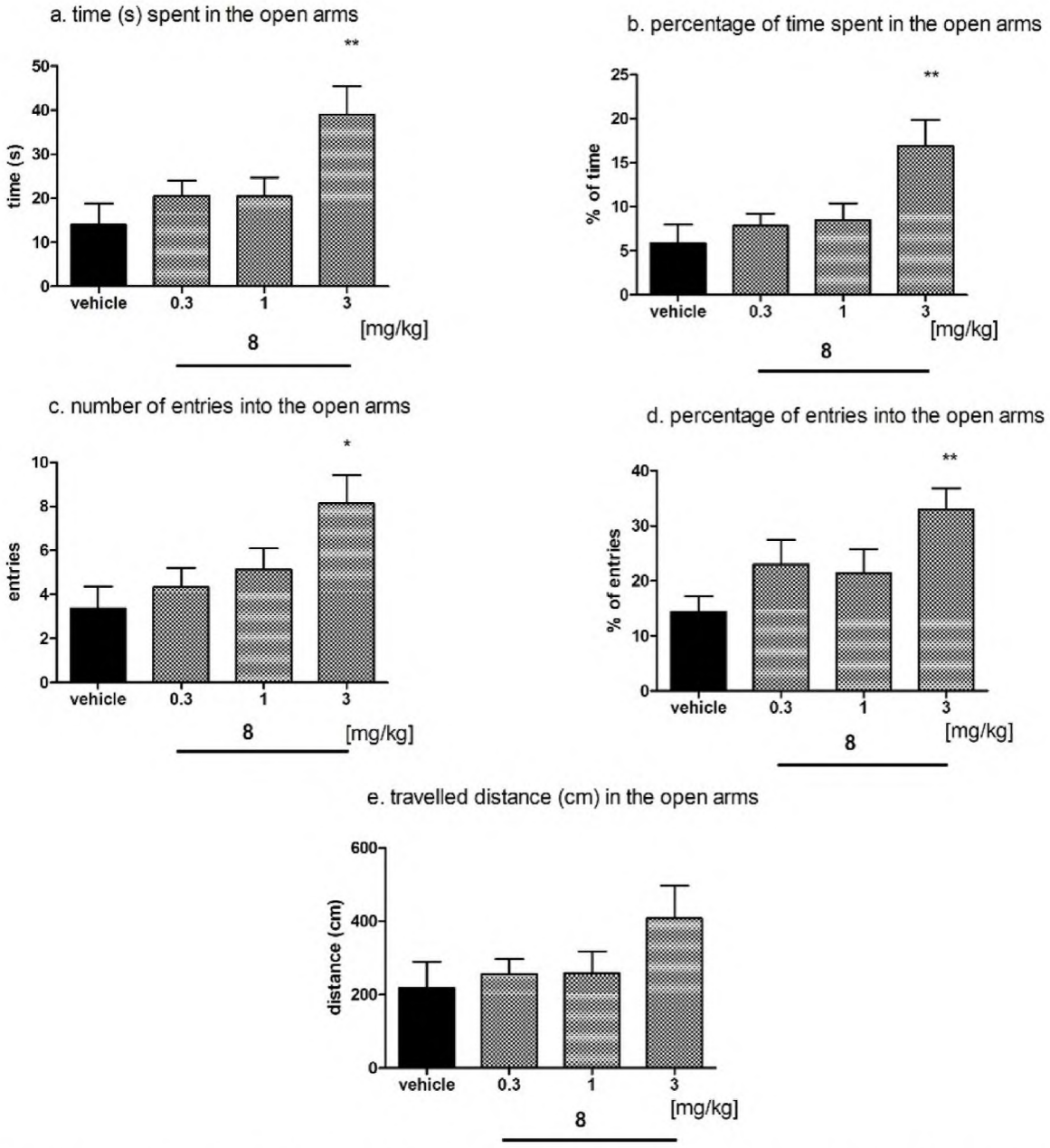

Fig. 16. Anxiolytic-like effects of compound **8** in the EPM test. Increased open-arm exploration denotes reduced anxiety. Compound **8** was given *i.p.* 60 min, before the test. Values represent the mean ± SEM of the time (a) and percentage of time (b) spent in the open arms and of entries (c) and percentage of entries (d) into the open arms (e) the travelled distance on the open arms during 5-min test session compared to the respective vehicle group *p < 0.05, **p < 0.01 (ANOVA is followed by the Bonferroni's post-hoc test); N = 6–8.

-F, -CF_3, and -OMe, respectively, at the phenyl ring, as well as an introduction of additional aromatic ring on the amine group.

In the case of the group of compounds **26-31**, the modification of lead **6** consisted of the introduction of an additional aromatic ring on the amino group at the 1,3,5-triazine to increase the lipophilicity of the compounds, as well as to capture an auxiliary protein target (CDK5) according to the computer-aided prediction. Although the latter goal was not achieved, the introduction of the additional phenyl ring allowed to maintain the strong affinities towards 5-HT_6R. In contrast, the introduction of the 4-pyridinyl group reduced this affinity without bringing the expected actions for additional targets (CDK5). Among this series, compound **31** proved to be the most active (K_i = 6 nM, Table 2). However, the druglikeness profile of this compound, in particular the water solubility, occurred less beneficial than that evaluated for its NH_2-unsubstituted analogues (**6** and **8**).

Indisputably, the presence of two fluorines in the 2,5-position occurred as the most beneficial for the 5-HT_6R affinity. The best receptor profile was observed for 2,5-difluorophenoxy-1,3,5-triazine derivative with a branched ethyl linker, compound **8** (K_i = 5 nM). The compound had a higher affinity for 5-HT_6R than olanzapine as well as strong nanomolar antagonistic activity (pK_b = 8.16, Table 3). Its antagonistic action was at the same level as that for compounds **10** and **14** containing also fluorine at position 2. A slightly weaker interaction can be observed for the 2-CF_3 substitution (compound **18**, pK_b = 7.69), which may be due to the excessive group size. In the case of the mixed substitution, *i.e.* one chlorine and one fluorine, or fluorine and -CF_3 group, the best arrangement was fluorine in the 2-position, and chlorine/-CF_3 in the 5-position of the aromatic ring. The double introduction

of the -CF_3 group resulted in a decrease in affinity for 5-HT_6R (**17**, **18**).

The introduction of two fluorine substituents at the phenyl ring in the place of two chlorine ones turned out highly beneficial for the drug-like properties of the tested 1,3,5-triazines due to the increase in lipophilicity and decrease of molecular weight. Higher lipophilicity seems to be desirable in term to penetrate across membrane barriers, including the blood-brain barrier, which is particularly important for compounds intended to act on the CNS. The 2,5-dichlorophenyl derivative **6** showed high permeability (*Pe* ca. 18 $*10^{-6}$ cm/s) in *in vitro* studies, but unfortunately had a risk of hepatotoxicity and was metabolically unstable. The 2,5-difluoro-analogue of the lead **6** found in this study, *i.e.* compound **8**, showed excellent metabolic stability and negligible hepatotoxicity risk, compared to **6** and its analogue with additional aromatic ring (**31**). Among the 1,3,5-triazine 5-HT_6R agents investigated so far, it was only one, the phenyl-unsubstituted analogue of **6** and **8**, which showed the comparably high metabolic stability with compound **8**, but a distinctly less potent affinity for 5-HT_6R [27].

Moreover, a significant ability to reverse MK-801-induced memory impairments of 2,5-difluorophenyl derivative **8** was observed in the NOR test in rats. The compound **8** was active even while administered in such a low dose as 0.3 mg/kg, and the active dose of **8** was significantly lower than that of the 2,5-dichlorosubstituted lead **6** [26] and the most of 5-HT_6R agents described to date [2]. Additionally, anxiolytic-like properties were demonstrated in the EPM test for compound **8**. In this test, strong pharmacological activity was observed only for the highest dose (3 mg/kg), but its effectivenes was much higher than that obtained for the previously investigated 1,3,5-triazine derivatives [27]. The observed impact on the memory processes and the anxiolytic-like effect of compound **8** *in vivo* appear to be due to a combination of factors, such as: *(i)* the highly potent 5-HT_6R antagonistic action, *(ii)* the very good membrane penetration (high permeability confirmed by the PAMPA assay), and *(iii)* the beneficial metabolic stability. Furthermore, the 2,5-difluorophenyloxy derivative **8** exerted a promising additional antiplatelet effect, giving an optimistic perspective of dual therapeutic effects that not only improve cognitive abilities but also prevents atherosclerotic lesions in elderly patient with AD.

4. Conclusions

The series of 1,3,5-triazine derivatives outlined herein extended the original family of potent 5-HT_6R antagonists, structurally distinct from the widely explored sulfone and indole-like compounds. The conducted studies allowed to identify a series of twenty-five new highly active 5-HT_6R agents, in particular, to find out a new "hit", *4-[1-(2,5-difluorophenoxy)propyl]-6-(4-methylpiperazin*-1-yl*)-1,3,5-triazin-2-amine* (**8**), which showed potent 5-HT_6R antagonistic activity in functional tests, significant *in vivo* procognitive/anxiolytic-like effects in rats, very good permeability in the PAMPA model and satisfactory safety in preliminary *in vitro* studies. All compounds obtained showed a very strong affinity towards the 5-HT_6R and significant selectivity for off-targets. SAR studies along the whole series, supported by crystallographic studies and molecular modelling, confirmed the beneficial effect of fluorine substitution for strong interaction with the 5-HT_6R target. Although the not-yet considered modification of the triazine at position 2 with an additional aromatic ring did not bring actions on desirable additional targets, it is worth noting that activity on 5-HT_6R was retained to open a 'new door' for further modifications at this triazine fragment in a search for interactions with other targets pertinent to AD therapy. Additionally, it is worth emphasizing the antiplatelet effect of compound **8** that was confirmed in this work. This offers a possibility of innovative cardiovascular-friendly therapy for older AD patients, in which compound **8** may be a starting point for further pharmacomodulation in a search of such dual actions.

Summing up, these comprehensive studies allowed to elect the most promising structure, compound **8**, among the series of novel and highly active serotonin receptor ligands, which will serve as a new leader useful in further search for 5-HT_6R agents with potential application in the treatment of cognitive disorders, particularly those associated with AD.

5. Experimental

5.1. Chemistry

Reagents were manufactured by Alfa Aesar (Karlsruhe, Germany) or Sigma Aldrich (Darmstadt, Germany). Dry solvents (stored under argon) were used. Reaction progress was monitored using thin-layer chromatography (TLC), which was performed on pre-coated Merck silica gel 60 F254 aluminum plates (Hex/EtOAc 4:1 for the formation of ester intermediates, DCM/MeOH 95:5 for the final step). Spots were visualized by UV light or treatment with Dragendorff reagent. Magnetic stirrer with a contact thermometer Heidolph MR 2001 was used to provide reactions at a fixed temperature. Intermediates (**33–51**) were obtained according to previously reported methods [26], and used as a crude form (purity 90–100%) for the final step (compounds **7–25**). More detailed descriptions of the finals and intermediates (**33–51**) are included in the Supplementary Material (see unit 1–2).

Melting points (mp) for final compounds were determined using MEL-TEMP II apparatus and are uncorrected. ^{1}H NMR, ^{19}F NMR and ^{13}C NMR spectra were recorded on a Varian Mercury-VX 500 MHz PFG instrument (Varian Inc, Palo Alto, CA) in DMSO-d_6 for all final compounds at ambient temperature. Chemical shifts values are expressed as δ values in (ppm) and the coupling constants (J) in Hz. Data are presented as follows: chemical shift, multiplicity (s, singlet; br. s, broad singlet; d, doublet; t, triplet; dd, doublet of doublet, q, quartet, qu, quintet, m, multiplet), coupling constant J, number of protons. Mass spectra obtained using UPLC-MS/MS system consisted of a Waters ACQUITY® UPLC® (Waters Corporation, Milford, MA, USA) combined with a Waters TQD mass spectrometer (electrospray ionization mode ESI-tandem quadrupole). The purity of all finals was established by UPLC/MS to be above 95%. Retention time values (t_R) are reported in minutes. HRMS mass spectra obtained by using the UPLC-QTof system consisted of a Waters Acquity I-Class Plus (Waters Corporation, Milford, MA, USA) coupled to a Waters Synapt XS mass spectrometer (electrospray ionization mode ESI). Data acquisition software was MassLynx V 4.2 (Waters).

5.1.1. General synthetic pathway for final compounds 7-25

Dissolution of sodium (10 mmol) in 10 ml of absolute methanol was followed by adding 4-methylpiperazine-1-yl biguanide hydrochloride (**32**) (5 mmol) and an appropriate ester (**33–51**, 5 mmol). The reaction mixture was carried out in reflux for 16 h. After cooling down, water (10 ml) was added and the reaction mixture was stirred for 30 min at room temperature. The precipitated product was filtered and crystallized from methanol to give a solid (method A) or was converted into hydrochloric salt form by addition of solution of HCl in diethyl ether (method B).

5.1.1.1. (RS)-4-(1-(2,5-difluorophenoxy)ethyl)-6-(4-methylpiperazin-1-yl)-1,3,5-triazin-2-amine (7). Ester **33**, reaction time: 16 h. Method A. White solid. Yield 58%, LC/MS^+ purity: 100%, t_R = 3.36, LC-HRMS/MS $[M+H]^+$ 351.1750, mp = 105–107 °C, $C_{16}H_{20}F_2N_6O$ (MW = 350.37). ^{1}H NMR (500 MHz, DMSO-d_6) δ [ppm]: 7.25–7.19 (m, 1H, Ar-4-H), 7.07 (br. s, 1H, Ar-NH), 6.91 (br. s, 1H, Ar-NH), 6.90–6.85 (m, 1H, Ar-3-H), 6.74–6.68 (m, 1H, Ar-6-H), 5.03 (q, J = 7.0 Hz, 1H, CH), 3.70–3.60 (m, 4H, Pp-2,6-H), 2.30–2.19 (m, 4H, Pp-3,5-H), 2.16 (s, 3H, N-CH_3), 1.55 (d, J = 3.8 Hz, 3H, CH_3). ^{13}C NMR (126 MHz, DMSO-d_6) δ [ppm]: 176.04, 167.49, 164.87, 159.40, 157.50, 147.25, 117.02, 107.00, 104.13, 77.45, 54.73, 46.25, 42.82, 20.39. ^{19}F NMR (471 MHz, DMSO-d_6) δ [ppm]: −116.37, −138.92.

5.1.1.2. (RS)-4-(1-(2,5-difluorophenoxy)propyl)-6-(4-methylpiperazin-1-yl)-1,3,5-triazin-2-amine (8). Ester **34**, reaction time: 16 h. Method A.

White solid. Yield 50%, LC/MS$^+$ purity: 100%, t_R = 3.85, LC-HRMS/MS $[M+H]^+$ 365.1917, mp = 130–132 °C, $C_{17}H_{22}F_2N_6O$ (MW = 364.40). ^{1}H NMR (500 MHz, DMSO-d_6) δ [ppm]: 7.25–7.19 (m, 1H, Ar-4-H), 7.06 (br. s, 1H, Ar-NH), 6.91 (br. s, 1H, Ar-NH), 6.88–6.83 (m, 1H, Ar-3-H), 6.74–6.69 (m, 1H, Ar-6-H), 4.78 (t, J = 8.3 Hz, 1H, CH), 3.70–3.61 (m, 4H, Pp-2,6-H), 2.29–2.20 (m, 4H, Pp-3,5-H), 2.16 (s, 3H, *N*-CH3), 1.95 (qu, J = 7.3 Hz, 2H, CH_2), 0.97 (t, J = 7.5 Hz, 3H, CH_3). ^{13}C NMR (126 MHz, DMSO-d_6) δ [ppm]: 175.31, 167.42, 164.83, 159.38, 157.48, 147.56, 116.95, 107.12, 104.36, 82.49, 54.73, 46.26, 42.81, 27.51, 10.27. ^{19}F NMR (471 MHz, DMSO-d_6) δ [ppm]: −116.35, −139.14.

*5.1.1.3. (RS)-4-(1-(5-chloro-2-fluorophenoxy)ethyl)-6-(4-methylpiperazin-1-yl)-1,3,5-triazin-2-amine (**9**).* Ester **35**, reaction time: 16 h. Method A. White solid. Yield 38%, LC/MS$^+$ purity: 100%, t_R = 3.82, LC-HRMS/MS $[M+H]^+$ 367.1438, mp = 142–143 °C, $C_{16}H_{20}ClFN_6O$ (MW = 366.83). ^{1}H NMR (500 MHz, DMSO-d_6) δ [ppm]: 7.26–7.21 (m, 1H, Ar-4-H), 7.13–7.05 (m, 2H, Ar-3-H, NH), 6.98–6.89 (m, 2H, Ar-6-H, NH), 5.06 (q, J = 6.5 Hz, 1H, CH), 3.65 (s, 4H, Pp-2,6-H), 2.25 (s, 4H, Pp-3,5-H), 2.16 (s, 3H, *N*-CH_3), 1.55 (d, J = 6.1 Hz, 3H, CH_3). ^{13}C NMR (126 MHz, DMSO-d_6) δ [ppm]: 175.97, 167.50, 164.84, 152.15, 150.21, 147.23, 128.41, 121.14, 117.88, 116.74, 77.50, 54.75, 46.27, 20.42. ^{19}F NMR (471 MHz, DMSO-d_6) δ [ppm]: −135.39.

5.1.1.4. (RS)-4-(1-(5-chloro-2-fluorophenoxy)propyl)-6-(4-methylpiperazin-1-yl)-1,3,5-triazin-2-amine (10). Ester **36**, reaction time: 16 h. Method A. White solid. Yield 36%, LC/MS$^+$ purity: 100%, t_R = 4.30, LC-HRMS/MS $[M+H]^+$ 381.1597, mp = 104–105 °C, $C_{17}H_{22}ClFN_6O$ (MW = 380.85). ^{1}H NMR (500 MHz, DMSO-d_6) δ [ppm]: 7.22–7.17 (m, 1H, Ar-4-H), 7.07–7.00 (m, 2H, Ar-3-H, NH), 6.93–6.85 (m, 2H, Ar-6-H, NH), 4.77 (t, J = 5.5 Hz, 1H, CH), 3.61 (s, 4H, Pp-2,6-H), 2.22 (s, 4H, Pp-3,5-H), 2.12 (s, 3H, *N*-CH_3), 1.91 (qu, J = 7.2 Hz, 2H, CH_2), 0.92 (t, J = 4.6 Hz, 3H, CH_3). ^{13}C NMR (126 MHz, DMSO-d_6) δ [ppm]: 175.25, 167.44, 164.79, 152.20, 150.26, 147.53, 128.40, 121.12, 117.89, 116.76, 82.55, 54.75, 46.27, 27.51, 10.26. ^{19}F NMR (471 MHz, DMSO-d_6) δ [ppm]: −135.56.

5.1.1.5. (RS)-4-(1-(2-chloro-5-fluorophenoxy)ethyl)-6-(4-methylpiperazin-1-yl)-1,3,5-triazin-2-amine hydrochloride (11). Ester **37**, reaction time: 16 h. Method B. White solid. Yield 45%, LC/MS + purity: 98.8%, t_R = 3.98, LC-HRMS/MS $[M+H]^+$ 367.1438, mp = 132–134 °C, $C_{16}H_{21}Cl_2FN_6O$ (MW = 366.83). ^{1}H NMR (500 MHz, DMSO-d_6) δ [ppm]: 11.69 (s, 1H, H^+), 7.83 (br. s, 1H, Ar-NH), 7.64 (br. s, 1H, Ar-NH), 7.49–7.43 (m, 1H, Ar-3-H), 7.06–7.00 (m, 1H, Ar-6-H), 6.86–6.80 (m, 1H, Ar-4-H), 5.34–5.23 (m, 2H, Pp-6-H), 5.22–5.17 (m, 1H, CH), 4.67–4.48 (m, 2H, Pp-2-H), 3.48–3.41 (m, 2H, Pp-5-H), 3.11–2.95 (m, 2H, Pp-3-H), 2.71 (s, 3H, *N*-CH_3), 1.62 (d, J = 6.8 Hz, 3H, CH_3). ^{13}C NMR (126 MHz, DMSO-d_6) δ [ppm]: 163.70, 162.66, 160.72, 154.68, 131.32, 118.00, 109.35, 104.35, 76.38, 52.87, 51.80, 42.44, 19.99. ^{19}F NMR (471 MHz, DMSO-d_6) δ [ppm]: −111.91.

5.1.1.6. (RS)-4-(1-(2-chloro-5-fluorophenoxy)propyl)-6-(4-methylpiperazin-1-yl)-1,3,5-triazin-2-amine (12). Ester **38**, reaction time: 16 h. Method A. White solid. Yield 35%, LC/MS + purity: 100%, t_R = 4.49, LC-HRMS/MS $[M+H]^+$ 381.1597, mp = 146–148 °C, $C_{17}H_{22}$ $ClFN_6O$ (MW = 380.85). ^{1}H NMR (500 MHz, DMSO-d_6) δ [ppm]: 7.65–7.61 (m, 1H, Ar-3-H), 7.46–7.42 (m, 1H, Ar-6-H), 7.33–7.26 (m, 1H, Ar-4-H), 6.99 (br. s, 1H, Ar-NH), 6.88 (br. s, 1H, Ar-NH), 4.01 (dd, J_1 = 8.6, J_2 = 6.0 Hz, 1H, CH), 3.62 (br. s, 4H, Pp-2,6-H), 2.26 (br. s, 4H, Pp-3,5-H), 2.17 (s, 3H, *N*-CH_3), 2.09–1.99 (m, 1H, CH), 1.92–1.83 (m, 1H, CH), 0.93 (t, J = 7.4 Hz, 3H, CH_3). ^{13}C NMR (126 MHz, DMSO-d_6) δ [ppm]: 176.31, 167.46, 164.73, 153.59, 138.72, 132.56, 129.94, 128.77, 127.84, 115.84, 108.88, 54.24, 46.29, 26.62, 12.30. ^{19}F NMR (471 MHz, DMSO-d_6) δ [ppm]: −112.28.

5.1.1.7. (RS)-4-(1-(2-fluoro-5-(trifluoromethyl)phenoxy)ethyl)-6-(4-methylpiperazin-1-yl)-1,3,5-triazin-2-amine (13). Ester **39**, reaction time: 16 h. Method A. White solid. Yield 45%, LC/MS + purity: 95.3%, t_R = 4.22, LC-HRMS/MS $[M+H]^+$ 401.1713, mp = 118–120 °C, $C_{17}H_{20}F_4N_6O$ (MW = 400.48). ^{1}H NMR (500 MHz, DMSO-d_6) δ [ppm]: 7.51–7.39 (m, 2H, Ar-3,4-H), 7.32–7.26 (m, 1H, Ar-6-H), 7.09 (br. s, 1H, Ar-NH), 6.92 (br. s, 1H, Ar-NH), 5.20–5.12 (m, 1H, CH), 3.77–3.51 (m, 4H, Pp-2,6-H), 2.31–2.17 (m, 4H, Pp-3,5-H), 2.15 (s, 3H, *N*-CH_3), 1.59 (d, J = 6.8 Hz, 3H, CH_3). ^{13}C NMR (126 MHz, DMSO-d_6) δ [ppm]: 175.84, 167.52, 164.77, 155.31, 153.34, 146.94, 125.28, 123.12, 117.44, 113.68, 77.72, 54.70, 46.24, 42.89, 20.26. ^{19}F NMR (471 MHz, DMSO-d_6) δ [ppm]:− 60.49, −127.60.

5.1.1.8. (RS)-4-(1-(2-fluoro-5-(trifluoromethyl)phenoxy)propyl)-6-(4-methylpiperazin-1-yl)-1,3,5-triazin-2-amine (14). Ester **40**, reaction time: 16 h. Method A. White solid. Yield 48%, LC/MS$^+$ purity: 100%, t_R = 4.57, LC-HRMS/MS $[M+H]^+$ 415.1870, mp = 132–134 °C, $C_{18}H_{22}F_4N_6O$ (MW = 414.41). ^{1}H NMR (500 MHz, DMSO-d_6) δ [ppm]: 7.49–7.37 (m, 2H, Ar-3,4-H), 7.33–7.27 (m, 1H, Ar-6-H), 7.07 (br. s, 1H, Ar-NH), 6.91 (br. s, 1H, Ar-NH), 4.90 (t, 1H, CH), 3.78–3.53 (m, 4H, Pp-2,6-H), 2.22 (s, 4H, Pp-3,5-H), 2.15 (s, 3H, *N*-CH_3), 1.99 (qu, J = 7.3 Hz, 2H, CH_2), 0.98 (t, J = 7.3 Hz, 3H, CH_3). ^{13}C NMR (126 MHz, DMSO-d_6) δ [ppm]: 175.14, 167.49, 164.74, 147.23, 142.31, 125.28, 123.12, 118.95, 117.62, 113.67, 82.78, 54.71, 46.25, 27.37, 10.20. ^{19}F NMR (471 MHz, DMSO-d_6) δ [ppm]: −60.50, −127.77.

5.1.1.9. (RS)-4-(1-(5-fluoro-2-(trifluoromethyl)phenoxy)ethyl)-6-(4-methylpiperazin-1-yl)-1,3,5-triazin-2-amine (15). Ester **41**, reaction time: 16 h. Method A. White solid. Yield 21%, LC/MS + purity: 100%, t_R = 4.44, LC-HRMS/MS $[M+H]^+$ 401.1713, mp = 152–154 °C, $C_{17}H_{20}F_4N_6O$ (MW = 400.38). ^{1}H NMR (500 MHz, DMSO-d_6) δ [ppm]: 7.51–7.39 (m, 2H, Ar-3,6-H), 7.32–7.26 (m, 1H, Ar-4-H), 7.09 (br. s, 1H, Ar-NH), 6.92 (br. s, 1H, Ar-NH), 5.20–5.12 (m, 1H, CH), 3.77–3.51 (m, 4H, Pp-2,6-H), 2.32–2.17 (m, 4H, Ar-3,5-H), 2.15 (s, 3H, *N*-CH_3), 1.59 (d, J = 6.6 Hz, 3H, CH_3). ^{13}C NMR (126 MHz, DMSO-d_6) δ [ppm]: 176.35, 175.66, 167.49, 164.95, 164.82, 163.74, 105.30, 103.35, 103,12, 101.71, 77.30, 55.98, 54.67, 46.22, 20.22.^{19}F NMR (471 MHz, DMSO-d_6) δ [ppm]: −59.74, −104.78.

5.1.1.10. (RS)-4-(1-(5-fluoro-2-(trifluoromethyl)phenoxy)propyl)-6-(4-methylpiperazin-1-yl)-1,3,5-triazin-2-amine (16). Ester **42**, reaction time: 16 h. Method A. White solid. Yield 48%, LC/MS$^+$ purity: 99.4%, t_R = 4.83, LC-HRMS/MS $[M+H]^+$ 415.1870, mp = 144–146 °C, $C_{18}H_{22}F_4N_6O$ (MW = 414.41). ^{1}H NMR (500 MHz, DMSO-d_6) δ [ppm]: 7.68–7.64 (m, 1H, Ar-3-H), 7.05–6.91 (m, 2H, Ar-NH2), 6.91–6.84 (m, 2H, Ar-4,6-H), 4.93 (t, J = 6.8 Hz, 1H, CH), 3.68–3.53 (m, 4H, Pp-2,6-H), 2.30–2.06 (m, 4H, Pp-3,5-H), 2.14 (s, 3H. N-CH3), 2.00–1.91 (m, 2H, CH_2), 0.97 (t, J = 7.5 Hz, 3H, CH_3). ^{13}C NMR (126 MHz, DMSO-d_6) δ [ppm]: 175.72, 174.96, 167.41, 164.75, 158.72, 129.43, 125.11, 122.95, 107.32, 103.06, 81.83, 55.96, 54.66, 46.22, 27.41, 9.97. ^{19}F NMR (471 MHz, DMSO-d_6) δ [ppm]: −60.23, −104.77.

5.1.1.11. (RS)-4-(1-(2,5-bis(trifluoromethyl)phenoxy)ethyl)-6-(4-methylpiperazin-1-yl)-1,3,5-triazin-2-amine (17). Ester **43**, reaction time: 16 h. Method A. White solid. Yield 45%, LC/MS$^+$ purity: 99.4%, t_R = 4.93, LC-HRMS/MS $[M+H]^+$ 451.1670, mp = 125–127 °C, $C_{18}H_{20}F_6N_6O$ (MW = 450.39). ^{1}H NMR (500 MHz, DMSO-d_6) δ [ppm]: 7.88–7.79 (m, 1H, Ar-6-H), 7.49 (s, 1H, Ar-3-H), 7.44–7.37 (m, 1H, Ar-4-H), 6.99 (d, J = 9.0 Hz, 2H, Ar-NH_2), 5.35–5.24 (m, 1H, CH), 3.59 (br. s, 4H, Pp-2,6-H), 2.33–1.99 (m, 7H, Pp-3,5-H, *N*-CH_3), 1.64–1.53 (m, 3H, CH_3). ^{13}C NMR (126 MHz, DMSO-d_6) δ [ppm]: 175.46, 167.52, 164.74, 157.11, 134.34, 128.63, 124.85, 122.68, 117.36, 112.26, 77.66, 54.65, 49.12, 46.21, 42.91, 19.94. ^{19}F NMR (471 MHz, DMSO-d_6) δ [ppm]: −61.51, −61.92.

5.1.1.12. (RS)-4-(1-(2,5-bis(trifluoromethyl)phenoxy)propyl)-6-(4-methylpiperazin-1-yl)-1,3,5-triazin-2-amine (18). Ester **44**, reaction time: 16 h. Method A. White solid. Yield 42%, LC/MS$^+$ purity: 100%, $t_R = 5.44$, LC-HRMS/MS $[M+H]^+$ 465.1882, mp = 105–107 °C, $C_{19}H_{22}F_6N_6O$ (MW = 464.42). ^{1}H NMR (500 MHz, DMSO-d_6) δ [ppm]: 7.87–7.82 (m, 1H, Ar-6-H), 7.43–7.38 (m, 2H, Ar-3,4-H), 7.03–6.98 (d, $J = 9.1$ Hz, 2H, Ar-NH_2), 5.06 (t, $J = 6.3$ Hz, 1H, CH), 3.69–3.49 (m, 4H, Pp-2,6-H), 2.36–2.05 (m, 4H, Pp-3,5-H), 2.16 (s, 3H, *N*-CH_3), 2.03–1.97 (m, 2H, CH_2), 0.99 (t, $J = 6.7$ Hz, 3H, CH_3). ^{13}C NMR (126 MHz, DMSO-d_6) δ [ppm]: 174.81, 171.93, 167.46, 164.67, 157.30, 128.76, 124.85, 122.68, 117.25, 111.92, 100.00, 82.13, 54.50, 46.02, 27.25, 9.94. ^{19}F NMR (471 MHz, DMSO-d_6) δ [ppm]: −61.51, −61.92.

5.1.1.13. (RS)-4-(1-(5-fluoro-2-methoxyphenoxy)ethyl)-6-(4-methylpiperazin-1-yl)-1,3,5-triazin-2-amine (19). Ester **45**, reaction time: 16 h. Method A. White solid. Yield 48%, LC/MS$^+$ purity: 100%, $t_R = 3.17$, LC-HRMS/MS $[M+H]^+$ 363.1927, mp = 140–142 °C, $C_{17}H_{23}FN_6O_2$ (MW = 362.41). ^{1}H NMR (500 MHz, DMSO-d_6) δ [ppm]: 7.05 (br. s, 1H, Ar-NH), 6.93–6.89 (m, 1H, Ar-4-H), 6.88 (br. s, 1H, Ar-NH), 6.71–6.62 (m, 2H, Ar-3,6-H), 4.88 (q, $J = 6.4$ Hz, 1H, CH), 3.74 (s, 3H, *O*-CH_3), 3.66 (s, 4H, Pp-2,6-H), 2.26 (s, 4H, Pp-3,5-H), 2.17 (s, 3H, *N*-CH_3), 1.52 (d, $J = 6.5$ Hz, 3H, CH_3). ^{13}C NMR (126 MHz, DMSO-d_6) δ [ppm]: 176.67, 167.53, 164.96, 157.55, 155.68, 148.79, 146.14, 113.29, 106.44, 103.14, 77.25, 56.59, 54.78, 46.28, 20.62. ^{19}F NMR (471 MHz, DMSO-d_6) δ [ppm]: −121.37.

5.1.1.14. (RS)-4-(1-(5-fluoro-2-methoxyphenoxy)propyl)-6-(4-methylpiperazin-1-yl)-1,3,5-triazin-2-amine (20). Ester **46**, reaction time: 16 h. Method A. White solid. Yield 38%, LC/MS$^+$ purity: 100%, $t_R = 3.62$, LC-HRMS/MS $[M+H]^+$ 377.2097, mp = 138–140 °C, $C_{18}H_{25}FN_6O_2$ (MW = 376.44). ^{1}H NMR (500 MHz, DMSO-d_6) δ [ppm]: 7.04 (br. s, 1H, Ar-NH), 6.93–6.89 (m, 1H, Ar-4-H), 6.87 (br. s, 1H, Ar-NH), 6.71–6.61 (m, 2H, Ar-3,6-H), 4.63 (t, $J = 9.4$ Hz, 1H, CH), 3.74 (s, 3H, *O*-CH_3), 3.66 (s, 4H, Pp-2,6-H), 2.26 (s, 4H, Pp-3,5-H), 2.17 (s, 3H, *N*-CH_3), 1.93–1.89 (m, 2H, CH_2), 0.96 (t, $J = 6.3$ Hz, 3H, CH_3). ^{13}C NMR (126 MHz, DMSO-d_6) δ [ppm]: 175.95, 167.45, 164.91, 157.58, 155.71, 149.25, 146.19, 113.51, 106.23, 103.16, 82.44, 56.75, 54.75, 46.28, 27.70, 10.47. ^{19}F NMR (471 MHz, DMSO-d_6) δ [ppm]: −121.27.

5.1.1.15. (RS)-4-(1-(2,3-difluorophenoxy)ethyl)-6-(4-methylpiperazin-1-yl)-1,3,5-triazin-2-amine (21). Ester **47**, reaction time: 16 h. Method A. White solid. Yield 45%, LC/MS$^+$ purity: 100%, $t_R = 3.46$, LC-HRMS/MS $[M+H]^+$ 351.1750, mp = 175–177 °C, $C_{16}H_{20}F_2N_6O$ (MW = 350.37). ^{1}H NMR (500 MHz, DMSO-d_6) δ [ppm]: 7.06–6.99 (m, 2H, Ar-5-H, NH), 6.97–6.85 (m, 2H, Ar-4-H, NH), 6.82–6.77 (m, 1H, Ar-6-H), 5.02 (q, $J = 6.6$ Hz, 1H, CH), 3.64 (br. s, 4H, Pp-2,6-H), 2.26 (br. s, 4H, Pp-3,5-H), 2.16 (s, 3H. *N*-CH_3), 1.56 (d, $J = 6.6$ Hz, 3H, CH_3). ^{13}C NMR (126 MHz, DMSO-d_6) δ [ppm]: 176.26, 167.45, 164.89, 148.10, 141.69, 139.85, 124.32, 111.95, 109.20, 77.55, 54.71, 46.26, 43.03, 20.66. ^{19}F NMR (471 MHz, DMSO-d_6) δ [ppm]: −138.47, −159.75.

5.1.1.16. (RS)-4-(1-(2,3-difluorophenoxy)propyl)-6-(4-methylpiperazin-1-yl)-1,3,5-triazin-2-amine (22). Ester **48**, reaction time: 16 h. Method A. White solid. Yield 34%, LC/MS$^+$ purity: 100%, $t_R = 3.97$, LC-HRMS/MS $[M+H]^+$ 365.1917, mp = 132–134 °C, $C_{17}H_{22}F_2N_6O$ (MW = 364.40). ^{1}H NMR (500 MHz, DMSO-d_6) δ [ppm]: 7.06–6.99 (m, 2H, Ar-5-H, NH), 6.96–6.84 (m, 2H, Ar-4-H, NH), 6.81–6.75 (m, 1H, Ar-6-H), 4.80–4.75 (m, 1H, CH), 3.64 (br. s, 4H, Pp-2,6-H), 2.25 (br. s, 4H, Pp-3,5-H), 2.16 (s, 3H, *N*-CH_3), 1.98–1.90 (m, 2H, CH_2), 1.01–0.96 (t, $J = 6.8$ Hz, 3H, CH_3). ^{13}C NMR (126 MHz, DMSO-d_6) δ [ppm]: 175.52, 167.38, 164.84, 150.05, 148.38, 139.80, 124.39, 111.97, 109.33, 82.60, 54.71, 46.26, 42.93, 27.77, 10.35. ^{19}F NMR (471 MHz, DMSO-d_6) δ [ppm]: −138.38, −159.94.

5.1.1.17. (RS)-4-(1-(3-chloro-2-fluorophenoxy)ethyl)-6-(4-methylpiperazin-1-yl)-1,3,5-triazin-2-amine (23). Ester **49**, reaction time: 16 h. Method A. White solid. Yield 34%, LC/MS$^+$ purity: 100%, $t_R = 3.94$, LC-HRMS/MS $[M+H]^+$ 367.1438, mp = 178–180 °C, $C_{16}H_{20}ClFN_6O$ (MW = 366.83). ^{1}H NMR (500 MHz, DMSO-d_6) δ [ppm]: 7.09–7.00 (m, 3H, Ar-4,5-H, NH), 6.98–6.92 (m, 1H, Ar-6-H), 6.89 (br. s, 1H, Ar-NH), 5.04 (q, $J = 7.9$ Hz, 1H, CH), 3.64 (br. s, 4H, Pp-2,6-H), 2.26 (br. s, 4H, Pp-3,5-H), 2.16 (s, 3H, *N*-CH_3), 1.56 (d, $J = 7.1$ Hz, 3H, CH_3). ^{13}C NMR (126 MHz, DMSO-d_6) δ [ppm]: 176.24, 167.46, 164.89, 149.22, 147.78, 125.31, 121.95, 120.86, 115.34, 100.00, 77.46, 54.73, 46.26, 20.66. ^{19}F NMR (471 MHz, DMSO-d_6) δ [ppm]: −136.10.

5.1.1.18. (RS)-4-(1-(3-chloro-2-fluorophenoxy)propyl)-6-(4-methylpiperazin-1-yl)-1,3,5-triazin-2-amine (24). Ester **50**, reaction time: 16 h. Method A. White solid. Yield 35%, LC/MS$^+$ purity: 99.4%, $t_R = 4.27$, LC-HRMS/MS $[M+H]^+$ 381.1597, mp = 170–172 °C, $C_{17}H_{22}ClFN_6O$ (MW = 380.85). ^{1}H NMR (500 MHz, DMSO-d_6) δ [ppm]: 7.09–7.00 (m, 3H, Ar-4,5-H, NH), 6.96–6.91 (m, 1H, Ar-6-H), 6.88 (br. s, 1H, Ar-NH), 4.79 (t, $J = 6.3$ Hz, 1H, CH), 3.64 (br. s, 4H, Pp-2,6-H), 2.26 (br. s, 4H, Pp-3,5-H), 2.16 (s, 3H, *N*-CH_3), 1.95 (qu, $J = 7.3$ Hz, 2H, CH_2), 0.98 (t, $J = 7.0$ Hz, 3H, CH_3). ^{13}C NMR (126 MHz, DMSO-d_6) δ [ppm]: 175.48, 167.38, 164.84, 149.26, 148.00, 147.31, 125.32, 121.94, 120.85, 115.36, 82.50, 54.72, 46.27, 27.76, 10.36. ^{19}F NMR (471 MHz, DMSO-d_6) δ [ppm]: −136.28.

5.1.1.19. (RS)-4-(1-(2-chloro-3-fluorophenoxy)propyl)-6-(4-methylpiperazin-1-yl)-1,3,5-triazin-2-amine (25). Ester **51**, reaction time: 16 h. Method A. White solid. Yield 48%, LC/MS$^+$ purity: 100%, $t_R = 4.35$, LC-HRMS/MS $[M+H]^+$ 381.1597, mp = 123–125 °C, $C_{17}H_{22}ClFN_6O$ (MW = 380.85). ^{1}H NMR (500 MHz, DMSO-d_6) δ [ppm]: 7.25–7.19 (m, 1H, Ar-5-H), 7.07–6.99 (m, 1H, Ar-NH), 6.96–6.91 (m, 1H, Ar-4-H), 6.88 (br. s, 1H, Ar-NH), 6.76–6.73 (m, 1H, Ar-6-H), 4.78 (t, $J = 8.7$ Hz, 1H, CH), 3.64 (br. s, 4H, Pp-2,6-H), 2.32–2.20 (m, 4H, Pp-3,5-H), 2.16 (s, 3H, *N*-CH_3), 2.00–1.93 (m, 2H, CH_2), 1.02 (t, $J = 7.4$ Hz, 3H, CH_3). ^{13}C NMR (126 MHz, DMSO-d_6) δ [ppm]: 175.58, 167.41, 164.84, 157.83, 155.97, 128.57, 110.88, 109.39, 108.86, 82.64, 54.73, 52.75, 46.26, 27.91, 10.38. ^{19}F NMR (471 MHz, DMSO-d_6) δ [ppm]: −114.64.

*5.1.2. General procedure for final compounds **26-31***

Compounds **26–31** were obtained in Buchwald_Hartwig reaction *via* reaction of the earlier synthesized dichlorophenoxy-1,3,5-triazine derivatives (**6**, **52–54**) [32] with bromobenzene or 4-bromopyridine, in the presence of sodium *tert*-butoxide and RuPhos Pd G3. An appropriate 1,3,5-triazine (0.25 mmol) and bromide (bromobenzene/4-bromopyridine 0.25 mmol) were dissolved in anhydrous 1,4-dioxane (5 ml) and sodium *tert*-butoxide (0.50 mmol) was added to the reaction mixture. Reaction mixture was purged with argon and followed by adding a catalyst (0.03 mmol). Reaction was carried out at 100 °C for 3h. Reaction mixture was filtered through Cellite and washed with ethyl acetate (20 ml). Filtrate was concentrated *in vacuo* and purified on flash chromatography (DCM/MeOH 9:1). Residue after flash was lyophilized.

5.1.2.1. 4-(1-(3,5-dichlorophenoxy)propyl)-6-(4-methylpiperazin-1-yl)-N-phenyl-1,3,5-triazin-2-amine (26). Starting material: *4-(1-(3,5-dichlorophenoxy)propyl)-6-(4-methylpiperazin*-1-yl*)-1,3,5-triazin-2-amine* (**52**), bromobenzene CAS: 108-86-1, reaction time: 3h. White solid. Yield: 41%, LC/MS$^+$ purity: 98%, $t_R = 1.39$, LC-HRMS/MS $[M+H]^+$ 473.1630, mp = 133–135 °C, $C_{23}H_{26}Cl_2N_6O$ (MW = 473.40). ^{1}H NMR (400 MHz, DMSO-d_6) δ [ppm]: 9.74 (s, 1H, Ar-NH), 7.63 (s, 2H, Ph-2,6-H), 7.30–7.22 (m, 2H, Ph-3,5-H), 7.13 (t, $J = 1.8$ Hz, 1H, Ph-4-H), 7.04 (d, $J = 1.8$ Hz, 2H, Ar-2,6-H), 6.98 (t, $J = 7.4$ Hz, 1H, Ar-4-H), 4.95 (s, 1H, CH), 3.75 (s, 4H, Pp-2,6-H), 2.39–2.27 (m, 4H, Pp-3,5-H), 2.20 (s, 3H, *N*-CH_3), 2.07–1.91 (m, 2H, CH2), 1.00 (t, $J = 7.4$ Hz, 3H, CH_3). ^{13}C NMR (126 MHz, DMSO-d_6) δ [ppm]: 175.55, 164.36, 160.30, 156.67, 139.86, 134.91, 128.99, 122.90, 120.44, 115.18, 70.96, 54.70, 46.22,

43.27, 27.55, 10.30.

5.1.2.2. 4-(1-(3,5-dichlorophenoxy)propyl)-6-(4-methylpiperazin-1-yl)-N-(pyridin-4-yl)-1,3,5-triazin-2-amine (27). Starting material: *4-(1-(3,5-dichlorophenoxy)propyl)-6-(4-methylpiperazin*-1-yl*)-1,3,5-triazin-2-amine* (**52**), 4-bromopyridine CAS: 1120-87-2, reaction time: 3h. White solid. Yield: 32%, LC/MS$^+$ purity: 94%, t_R = 1.14, LC-HRMS/MS $[M+H]^+$ 474.1583, mp = 129–131 °C, $C_{22}H_{25}Cl_2N_7O$ (MW = 474.39). ^{1}H NMR (400 MHz, DMSO-d_6) δ [ppm]: 10.13 (s, 1H, Ar-NH), 8.38–8.32 (m, 2H, Ph-3,5-H), 7.67–7.61 (m, 2H, Ph-2,6-H), 7.13 (t, J = 1.8 Hz, 1H, Ar-4-H), 7.06 (d, J = 1.8 Hz, 2H, Ar-2,6-H), 5.04 (s, 1H, CH), 3.81–3.77 (m, 4H, Pp-2,6-H), 2.40–2.29 (m, 4H, Pp-3,5-H), 2.21 (s, 3H, *N*-CH_3), 2.10–1.93 (m, 2H, CH_2), 1.01 (t, J = 7.4 Hz, 3H, CH_3).

5.1.2.3. 4-(1-(3,5-dichlorophenoxy)pentyl)-6-(4-methylpiperazin-1-yl)-N-phenyl-1,3,5-triazin-2-amine (28). Starting material: *4-(1-(3,5-dichlorophenoxy)pentyl)-6-(4-methylpiperazin*-1-yl*)-1,3,5-triazin-2-amine* (**53**), bromobenzene CAS: 108-86-1, reaction time: 3h. White solid. Yield: 27%, LC/MS$^+$ purity: 96%, t_R = 1.46, LC-HRMS/MS $[M+H]^+$ 501.1973, mp = 135–137 °C, $C_{25}H_{30}Cl_2N_6O$ (MW = 501.46). ^{1}H NMR (400 MHz, DMSO-d_6) δ [ppm]: 9.74 (s, 1H, Ar-NH), 7.63 (s, 2H, Ph-2,6-H), 7.30–7.22 (m, 2H, Ph-3,5-H), 7.12 (t, J = 1.8 Hz, 1H, Ph-4-H), 7.03 (d, J = 1.8 Hz, 2H, Ar-2,6-H), 6.98 (t, J = 7.4 Hz, 1H, Ar-4-H), 4.99 (s, 1H, CH), 3.75 (s, 4H, Pp-2,6-H), 2.38–2.27 (m, 4H, Pp-3,5-H), 2.20 (s, 3H, *N*-CH_3), 2.00–1.92 (m, 2H, CH_2), 1.53–1.40 (m, 2H, CH_2), 1.39–1.31 (m, 2H, CH_2), 0.89 (t, J = 7.1 Hz, 3H, CH_3). ^{13}C NMR (126 MHz, DMSO-d_6) δ [ppm]: 186.09, 175.74, 164.36, 139.86, 134.92, 128.98, 122.90, 120.44, 115.15, 87.13, 66.57, 54.74, 46.22, 27.58, 22.43, 14.39.

5.1.2.4. 4-(1-(3,5-dichlorophenoxy)pentyl)-6-(4-methylpiperazin-1-yl)-N-(pyridin-4-yl)-1,3,5-triazin-2-amine (29). Starting material: *4-(1-(3,5-dichlorophenoxy)pentyl)-6-(4-methylpiperazin*-1-yl*)-1,3,5-triazin-2-amine* (**53**), 4-bromopyridine CAS: 1120-87-2, reaction time: 3h. White solid. Yield: 37%, LC/MS$^+$ purity: 96%, t_R = 1.46, mp = 133–135 °C, $C_{24}H_{29}Cl_2N_7O$ (MW = 502.44). ^{1}H NMR (400 MHz, DMSO-d_6) δ [ppm]: 10.12 (s, 1H, Ar-NH), 8.34 (d, J = 5.5 Hz, 2H, Ph-3,5-H), 7.63 (d, J = 6.1 Hz, 2H, Ph-2,6-H), 7.12 (t, J = 1.8 Hz, 1H, Ar-4-H), 7.04 (d, J = 1.8 Hz, 2H, Ar-2,6-H), 5.07 (s, 1H, CH), 3.77 (s, 4H, Pp-2,6-H), 2.39–2.34 (m, 4H, Pp-3,5-H), 2.20 (s, 3H, *N*-CH_3), 2.01–1.94 (m, 2H, CH_2), 1.52–1.39 (m, 2H, CH_2), 1.38–1.30 (m, 2H, CH_2), 0.88 (t, J = 7.1 Hz, 3H, CH_3).

5.1.2.5. 4-(1-(2,3-dichlorophenoxy)propyl)-6-(4-methylpiperazin-1-yl)-N-phenyl-1,3,5-triazin-2-amine (30). Starting material: *4-(1-(2,3-dichlorophenoxy)propyl)-6-(4-methylpiperazin*-1-yl*)-1,3,5-triazin-2-amine* (**54**), bromobenzene CAS: 108-86-1, reaction time: 3h. White solid. Yield: 30%, LC/MS$^+$ purity: 94%, t_R = 7.48, LC-HRMS/MS $[M+H]^+$ 473.1630, mp = 130–132 °C, $C_{23}H_{26}Cl_2N_6O$ (MW = 473.40). ^{1}H NMR (500 MHz, DMSO-d_6) δ [ppm]: 9.91–9.58 (m, 1H, Ar-NH), 7.63 (s, 2H, Ph-2,6-H), 7.46 (d, J = 8.5 Hz, 1H, Ar-4-H), 7.23 (d, J = 13.0 Hz, 2H, Ph-3,5-H), 7.11 (d, J = 2.3 Hz, 1H, Ph-4-H), 7.01–6.94 (m, 2H, Ar-5,6-H), 5.10–4.91 (m, 1H, CH), 3.82–3.66 (m, 4H, Pp-2,6-H), 2.38–2.25 (m, 4H, Pp-3,5-H), 2.19 (s, 3H, *N*-CH_3), 2.09–1.99 (m, 2H, CH_2), 1.03 (t, J = 7.4 Hz, 3H, CH_3). ^{13}C NMR (126 MHz, DMSO-d_6) δ [ppm]: 175.71, 170.42, 164.32, 155.79, 139.92, 132.84, 128.92, 122.81, 120.93, 120.36, 113.71, 108.66, 103.71, 89.99, 54.65, 46.19, 43.32, 27.97, 10.35.

5.1.2.6. 4-(1-(2,5-dichlorophenoxy)propyl)-6-(4-methylpiperazin-1-yl)-N-phenyl-1,3,5-triazin-2-amine (31). Starting material: *4-(1-(2,5-dichlorophenoxy)propyl)-6-(4-methylpiperazin*-1-yl*)-1,3,5-triazin-2-amine* (**6**), bromobenzene CAS: 108-86-1, reaction time: 3h. White solid. Yield: 30%, LC/MS$^+$ purity: 94%, t_R = 7.45, LC-HRMS/MS $[M+H]^+$ 473.1630, mp = 127–129 °C, $C_{23}H_{26}Cl_2N_6O$ (MW = 473.40). ^{1}H NMR (500 MHz, DMSO-d_6) δ [ppm]: 9.77 (s, 1H, Ar-NH), 7.63 (s, 2H, Ph-2,6-H), 7.45 (d, J = 8.5 Hz, 1H, Ar-4-H), 7.30–7.18 (m, 2H, Ph-3,5-H), 7.10 (d, J = 2.3 Hz, 1H, Ar-3-H), 6.98 (dd, J_1 = 8.5, J_2 = 2.3 Hz, 1H, Ar-6-H), 6.95 (d, J = 8.1 Hz, 1H, Ph-4-H), 4.99 (s, 1H, CH), 3.81–3.65 (m, 4H, Pp-2,6-H), 2.37–2.24 (m, 4H, Pp-3,5-H), 2.18 (s, 3H, *N*-CH_3), 2.08–1.99 (m, 2H, CH_2), 1.02 (t, J = 7.4 Hz, 3H, CH_3). ^{13}C NMR (126 MHz, DMSO-d_6) δ [ppm]: 175.41, 164.40, 154.92, 139.91, 132.43, 131.49, 128.97, 122.84, 121.76, 121.14, 120.38, 115.62, 70.96, 54.63, 46.19, 43.38, 27.62, 22.48, 10.22.

5.2. Crystallographic analysis

Crystals of **22** were obtained from methanol by slow evaporation of the solvent under ambient conditions.

Intensity for a single crystal was collected using the XtaLAB Synergy-S diffractometer, with a mirror monochromator and microfocus CuKα radiation source (1.54184 Å). The phase problem was solved by direct methods using SHELXTL [54]. The parameters of the obtained model were refined by full-matrix least-squares on F^2 using SHELXL [55]. All nonhydrogen atoms were refined anisotropically. Hydrogen atoms attached to nitrogen atoms were located on the difference Fourier map and refined without any restraints. All hydrogen atoms bonded to carbon atoms were included in the structure at idealized positions and were refined using a riding model. The molecular graphics were generated with the MERCURY program [56].

Crystallographic data for **22**: $C_{17}H_{22}F_2N_6O$, M_r = 364.40, wavelength 1.54184 Å, crystal size = 0.12 x 0.21 × 0.32 mm^3, monoclinic, space group C2/c, a = 33.4685(2) Å, b = 6.86826(3) Å, c = 15.74179(8) Å, β = 90.3227(5)°, V = 3618.52(3) Å^3, Z = 8, T = 100(2) K, 60244 reflections collected, 3926 unique reflections (R_{int} = 0.0359), R1 = 0.0364, w*R*2 = 0.0941 [I > 2σ(I)], R1 = 0.0368, w*R*2 = 0.0943 [all data].

CCDC 2124761 contains the supplementary crystallographic data. These data can be obtained free of charge from The Cambridge Crystallographic Data Centre via www.ccdc.cam.ac.uk/data_request/cif.

5.3. Molecular modelling

In this study, the crystal structures of considered target proteins retrieved from the Protein Data Bank [67] were used: structure of 5-HT_6R in the complex with agonist serotonin (PDB ID: 7XTB) and CDK5 structure (PDB ID: 3O0G). 3D structures of the compounds **7–31**, as well as two reference compounds used in the CDK5-based modeling, were prepared using LigPrep, which performed an appropriate ionization states assignment at pH 7.4 ± 1.0 using Epik (Schrödinger, New York, NY, USA). On the other hand, the proteins were prepared using Protein Preparation Wizard (to assign the bond orders, check for steric clashes and assign appropriate amino acid ionization states). Standard Glide docking was used in the CDK5 modeling and induced fit docking (IFD) was applied in the 5-HT_6R study. In each case, the grid box with a size of 10 Å was centered on the co-crystallized ligand and extended conformation searching was performed.

5.4. GPCR binding profile

5.4.1. Radioligand binding assays

The assays were carried out according to previously described methods by our research group [23,26,57]. Details are presented in Supplementary Material.

5.4.2. Functional assays towards 5-HT_6R

The study was performed in the same way as that in the previous work [26,27]. More details are presented in Supplementary Material.

5.5. Enzyme inhibitory profile

5.5.1. CDK5/p25 activity measurement

The inhibition of CDK5/p25 enzyme was measured using CDK5/p25 Kinase Enzyme System (Promega) and ADP-Glo Kinase Assay kit (Promega) according to the manufacturer's recommendations [58]. The principle of the method works based on the CDK5/p25 reaction, which utilizes ATP and generates ADP. Then the ADP- Glo Reagent is added to simultaneously terminate the kinase reaction and deplete the remaining ATP. Finally, the Kinase Detection Reagent is added to convert ADP to ATP and the newly synthesized ATP is converted to light using the luciferase/luciferin reaction. ATP was involved in the kinase reaction of CDK5/p25 phosphorylating its substrate, histone H1. The amount of ADP formed in this reaction reflects the activity of CDK5/p25.

Tested and reference compounds were dissolved in dimethyl sulfoxide (DMSO) at a concentration of 10 mM. Serial dilutions of tested compounds and standard were prepared in a 96-well microplate in assay buffer (200 mM Tris-HCl, pH 7.5, 100 mM $MgCl_2$ and 0.5 μg/μl BSA) and 4 to 7 concentrations were tested.

The CDK5/p25 (human, recombinant full-length) enzyme was incubated with tested and reference compounds, ATP and histone H1 at 30 °C for 15 min. In the reaction, the concentration of ATP, CDK5/p25, and histone H1 in the mix reaction were 50 μM, 15 ng, and 0.1 μg/μl, respectively. After the end of incubation, ADP-Glo Reagent was added and incubated 40 min at 22 °C. Next, Kinase Detection Reagent was added. After 30 min of incubation at 22 °C, the luminescence was measured by using a multifunction plate reader (POLARstar Omega, BMG Labtech, Germany). All reactions were carried out in white-walled, 384-well plates which were obtained from PerkinElmer. The percentage of inhibition was calculated and IC_{50} was determined by nonlinear regression analysis using GraphPad Prism 6.0 software.

5.5.2. MAO-B inhibition screening

Inhibitor's activity was measured in the fluorometric method described before [8,34] using human recombinant MAO-B 0.05 U per well (Sigma Aldrich M7441, Darmstadt, Germany), substrate p-tyramine 200 μM (Alfa Aesar A12220, Ward Hill, Massachusetts, USA), with reference to inhibitors at 1 μM: reversible safinamide (Cayman Chemical, Ann Arbor, Michigan, USA) and irreversible rasagiline (Sigma Aldrich, Darmstadt, Germany). Compounds were tested in two concentrations (1 μM and 10 μM) and the results were normalized to solvent control (DMSO, no inhibition, 0%) and rasagiline 1 μM (fully inhibited enzyme, 100%). If compounds exceeded 50% of maximal inhibition they would be chosen for testing in a dose-dependent manner and IC_{50} would be calculated.

5.6. Safety in vitro

5.6.1. Reference compounds

The references applied in ADMETox studies *in vitro*: doxorubicin (DX), caffeine (CFN) and verapamil (VER) were purchased from Sigma-Aldrich (St. Louis, MO, USA).

5.6.2. Permeability

Compounds' passive transport through cell membranes was estimated using Pre-coated PAMPA Plate System Gentest™ provided by Corning (Tewksbury, MA, USA). The assay was carried out according to the manufacturer's instruction and was already described by our research group [26,27,40,41,45]. The permeability coefficient *Pe* was counted based on the equation provided by the supplier [45] after measurement of the concentrations in apical and basolateral wells using the LC/MS analysis with an internal standard. The results were compared to the high permeable reference CFN.

5.6.3. Hepatotoxicity

Hepatoma HepG2 (ATCC® HB-8065™) cells were used in the test to assess hepatotoxicity. Both the details of the assay and the conditions for cell growth have already been reported earlier [27,40,41]. Examined compounds were added to the cells and incubated for 72 h in the four concentrations: 1, 10, 50 and 100 μM. Results were compared to the reference toxin DX which was implemented at 1 μM. The cells' viability was defined by standard MTS Assay administered by Promega (Madison, WI, USA). Multifunctional reader EnSpire (PerkinElmer, Waltham, MA USA) was used to measure the absorbance at 490 nm.

5.6.4. Metabolic stability

Metabolic stability I phase assay consisted of incubation of compounds with rat liver microsomes (RLMs) for 120 min at 37 °C according to the previously revealed protocol [40,41].. The procedure for the Phase II metabolism test was as follows: 200 μl of reaction mixture in Eppendorf was prepared using 87 μl 100 mM Tris-HCl, 5 μl 100 mM $MgCl_2$ (2.5 mM in the essay), 10 μl 1 mM of compound **8** (50 μM in essay) and 8 μl microsomes (RLMs). Reaction mixture was subjected to preincubation at 37 °C for 5 min. Then added 40 μl of 10 mM UDPGA (2 mM in essay) and 50 μl of NAPDH. The control sample was 50 μM of 7-Hydroxycoumarin. Duration of reaction: 1h at 37 °C. After the reaction 200 μl of cold ACN was added and centrifuged on vortex. The supernatant solution was collected, diluted with ACN and logged for LC/MS analysis.

RLMs were purchased from (Sigma-Aldrich, St. Louis, MO, USA). The LC/MS analysis was used as a tool for potential metabolites determination. The procedure was supported by the *in silico* prediction of possible metabolic pathways by using MetaSite 8.0.1. Software (Molecular Discovery Ltd., Hertfordshire, UK).

5.7. In vitro aggregation test

In vitro aggregation tests were conducted using freshly drawn whole rat blood with a Multiplate platelet function analyzer (Roche Diagnostic, Mannheim, Germany) based on the measurements of electric impedance. Blood was drawn from rats' carotid arteries with hirudin blood tube (Roche Diagnostic, Mannheim, Germany). Anticoagulated blood (300 μL) was mixed with 300 μL of the prewarmed isotonic saline solution containing studied compound or vehicle (DMSO 0.1%) and preincubated for 3 min at 37 °C with continuous stirring. Aspirin (Tocris, Abingdon, UK) was used as a reference compound. Aggregation was induced by adding collagen (Hyphen-Biomed, France) at the final concentration of 1.6 μg/mL. Activated platelet function aggregation process was recorded for 6 min. The Multiplate software analyzed the area under the curve (AUC) of the clotting process for each measurement and calculated the mean values. Each concentration of studied compounds was tested at least three times. Concentration-inhibition curves were constructed and analyzed by non-linear curve fitting using GraphPad Prism 6.0 (GraphPad Software Inc., San Diego, CA, USA).

The results are expressed as mean ±Δ/2, where Δ is a width of the 95% confidence interval (CI). Statistically significant differences between groups were calculated using one-way analysis of variance (ANOVA) and the post-hoc Dunnett's test. The criterion for significance was set at $p < 0.05$.

5.8. In vivo studies

5.8.1. Animals

Eight-week-old male Wistar rats were obtained from an accredited animal facility at the Jagiellonian University Medical College, Poland. Approvals for the study was obtained from the I Local Ethics Commission in Cracow (no 309/2019, 17.07.2019). All applicable international, national and institutional guidelines for the care and use of animals were followed (the detailed information is included in Supplementary Material). A total of 152 rats weighing 200–260g were housed in a group of four in a controlled environment (the detailed information is included in Supplementary Material) and after 5 days acclimatization period were

divided into experimental groups (n = 6–8/group): (1) control rats injected with vehicle (1% Tween 80 (Sigma Aldrich, PL)), (2) 0.1 mg/kg of MK-801 injected rats (water solution of MK-801 maleate (Bio-Techne, PL)), (3) groups injected with selected doses of compound 8 jointly with MK-801 (0.1 mg/kg). All compounds were injected intraperitoneally (*i.p.*) in a volume of 2 mL/kg.

5.8.2. Novel object recognition (NOR) test

The protocol was adapted from the original work [59,60] and the test and the administration of compounds were done according to the previously described protocol (compound **8** and MK-801 were administered, 60 and 30 min, respectively, before the T1 phase (the familiarization phase)) [27]. The discrimination index (DI) was calculated according to the formula:

$$DI = \frac{(EB - EA)}{(EA + EB)}$$

EB – the exploration time of novel object during the T2 session
EA – the exploration time of familiar object during the T2 session

MK-801 was chosen as the memory disturbance-induced compound based on the literature data which indicates that selective 5-HT_6R antagonists may prevent memory disturbances in rats induced by MK-801 [27,61]. To assess the impact of the injected compounds on the rats' exploratory activity the total exploration time in the T2 phase was measured.

5.8.3. Forced swim test (FST)

The experiment was carried out according to the method of Porsolt [62] the procedure and administration of compounds was done according to the previously described protocol [27]. The immobility was assigned when no additional activity was observed other than that necessary to keep the rat's head above the water. Fresh water was used for each animal.

5.8.4. Elevated plus-maze test (EPM test)

The testing procedure was based on a method described by Pellow and File [63]. The procedure and administration of compounds were performed according to the protocol described previously [27] (details see in the Supplementary Material). The EPM test is an 'unconditional' anxiety test based on the natural aversion of rodents to heights and open space. The increase in open-arm exploration, observed in the EPM test after administration of investigated compounds, denotes reduced anxiety behavior in that model *vs* vehicle-treated animals.

5.8.5. Exploratory activity measured in the EPM test

The experiment was performed using an EPM apparatus (details see in the Supplementary Material) to discern drug effects on general activity from those on open-arm exploration, during a 5-min test period (*i.e.* the time equal to the observation period in the EPM test).

5.8.6. Statistical analysis

Results of *in vivo* studies are presented as mean ± standard error of the mean (SEM). The obtained data were evaluated by one-way ANOVA followed by Bonferroni's Comparison Test. Statistical analysis was performed using the Statistica 13 software (Statsoft, Inc., USA).

Declaration of competing interest

The authors declare that they have no known competing financial interests or personal relationships that could have appeared to influence the work reported in this paper.

Data availability

Data will be made available on request.

Acknowledgments

Authors thank Piotr Mazur for his technical support in synthetic work. This research was financially supported by the National Science Center grants: 2018/31/B/NZ7/02160 and 2020/37/N/NZ7/02792 (synthesis of compounds **26–31**, enzyme assays) and Jagiellonian University Medical College grant number N42/DBS/000287 (influence on platelet aggregation in vitro) and N42/DBS/000192 (ADMET in vitro). Part of the synthesis was done within the Student Medicinal Chemistry Scientific Group at the Department of Technology and Biotechnology of Drugs, JU MC (Studenckie Koło Chemii Medycznej, UJCM).

Appendix A. Supplementary data

Supplementary data to this article can be found online at https://doi.org/10.1016/j.ejmech.2023.115756.

References

[1] C. Ferrari, S. Sorbi, The complexity of Alzheimer's disease: an evolving puzzle, Physiol. Rev. 101 (2021) 1047–1081, https://doi.org/10.1152/PHYSREV.00015.2020.
[2] K. Kucwaj-Brysz, H. Baltrukevich, K. Czarnota, J. Handzlik, Chemical update on the potential for serotonin 5-HT_6 and 5-HT_7 receptor agents in the treatment of Alzheimer's disease, Bioorg. Med. Chem. Lett. 49 (2021), https://doi.org/10.1016/J.BMCL.2021.128275.
[3] S. Dhillon, Aducanumab: first approval, Drugs 81 (2021) 1437–1443, https://doi.org/10.1007/S40265-021-01569-Z.
[4] S.M. Hoy, Lecanemab: first approval, Drugs (2023), https://doi.org/10.1007/S40265-023-01851-2.
[5] G. Marucci, M. Buccioni, D.D. Ben, C. Lambertucci, R. Volpini, F. Amenta, Efficacy of acetylcholinesterase inhibitors in Alzheimer's disease, Neuropharmacology 190 (2021), https://doi.org/10.1016/J.NEUROPHARM.2020.108352.
[6] A. Zagórska, A. Jaromin, Perspectives for new and more efficient multifunctional ligands for Alzheimer's disease therapy, Molecules 25 (2020), https://doi.org/10.3390/molecules25153337.
[7] S.R. Alizadeh, M.A. Ebrahimzadeh, Pyrazolotriazines: biological activities, synthetic strategies and recent developments, Eur. J. Med. Chem. 223 (2021), https://doi.org/10.1016/J.EJMECH.2021.113537.
[8] V. Canale, K. Grychowska, R. Kurczab, M. Ryng, A.R. Keeri, G. Satała, A. Olejarz-Maciej, P. Koczurkiewicz, M. Drop, K. Blicharz, K. Piska, E. Pękala, P. Janiszewska, M. Krawczyk, M. Walczak, S. Chaumont-Dubel, A.J. Bojarski, P. Marin, P. Popik, P. Zajdel, A dual-acting 5-HT_6 receptor inverse agonist/MAO-B inhibitor displays glioprotective and pro-cognitive properties, Eur. J. Med. Chem. 208 (2020), https://doi.org/10.1016/J.EJMECH.2020.112765.
[9] Z. Özdemir, M.A. Alagöz, Ö.F. Bahçecioğlu, S. Gök, Monoamine oxidase-B (MAO-B) inhibitors in the treatment of alzheimer's and Parkinson's disease, Curr. Med. Chem. 28 (2021) 6045–6065, https://doi.org/10.2174/0929867328666210203204710.
[10] S.K. Kumar, B. LaPlant, W.J. Chng, J. Zonder, N. Callander, R. Fonseca, B. Fruth, V. Roy, C. Erlichman, A.K. Stewart, Dinaciclib, a novel CDK inhibitor, demonstrates encouraging single-agent activity in patients with relapsed multiple myeloma, Blood 125 (2015) 443–448, https://doi.org/10.1182/BLOOD-2014-05-573741.
[11] M. Gąssowska-Dobrowolska, A. Kolasa-Wołosiuk, M. Cieślik, A. Dominiak, K. Friedland, A. Adamczyk, Alterations in tau protein level and phosphorylation state in the brain of the autistic-like rats induced by prenatal exposure to valproic acid, Int. J. Mol. Sci. 22 (2021) 3209, https://doi.org/10.3390/ijms22063209.
[12] R. Shukla, T.R. Singh, Identification of small molecules against cyclin dependent kinase-5 using chemoinformatics approach for Alzheimer's disease and other tauopathies, J. Biomol. Struct. Dyn. (2020), https://doi.org/10.1080/07391102.2020.1844050.
[13] R. Roufayel, N. Murshid, CDK5: key regulator of apoptosis and cell survival, Biomedicines 7 (2019) 88, https://doi.org/10.3390/biomedicines7040088.
[14] C. Ao, C. Li, J. Chen, J. Tan, L. Zeng, The role of CDK5 in neurological disorders, Front. Cell. Neurosci. 16 (2022), https://doi.org/10.3389/FNCEL.2022.951202.
[15] G. Mushtaq, N.H. Greig, F. Anwar, F.A. Al-Abbasi, M.A. Zamzami, H.A. Al-Talhi, M. A. Kamal, Neuroprotective mechanisms mediated by CDK5 inhibition, Curr. Pharmaceut. Des. 5 (2016) 527–534.
[16] G.N. Patrick, L. Zukerberg, M. Nikolic, S. De La Monte, P. Dikkes, L.H. Tsai, Conversion of p35 to p25 deregulates CDK5 activity and promotes neurodegeneration, Nature 402 (1999) 615–622, https://doi.org/10.1038/45159.
[17] M.S. Lee, Y.T. Kwon, M. Li, J. Peng, R.M. Friedlander, L.H. Tsai, Neurotoxicity induces cleavage of p35 to p25 by calpain, Nature 405 (2000) 360–364, https://doi.org/10.1038/35012636.

[18] R. Nirogi, R. Abraham, V. Benade, R.B. Medapati, P. Jayarajan, G. Bhyrapuneni, N. Muddana, V.R. Mekala, R. Subramanian, A. Shinde, R. Kambhampati, V. Jasti, SUVN-502, a novel, potent, pure, and orally active 5-HT 6 receptor antagonist: pharmacological, behavioral, and neurochemical characterization, Behav. Pharmacol. 30 (2019) 16–35, https://doi.org/10.1097/FBP.0000000000000414.

[19] M. Kotańska, K. Lustyk, A. Bucki, M. Marcinkowska, J. Śniecikowska, M. Kołaczkowski, Idalopirdine, a selective 5-HT6 receptor antagonist, reduces food intake and body weight in a model of excessive eating, Metab. Brain Dis. 33 (2018) 733–740, https://doi.org/10.1007/s11011-017-0175-1.

[20] T. Fullerton, B. Binneman, W. David, M. Delnomdedieu, J. Kupiec, P. Lockwood, J. Mancuso, J. Miceli, J. Bell, A Phase 2 clinical trial of PF-05212377 (SAM-760) in subjects with mild to moderate Alzheimer's disease with existing neuropsychiatric symptoms on a stable daily dose of donepezil, Alzheimer's Res. Ther. 10 (2018), https://doi.org/10.1186/s13195-018-0368-9.

[21] J. Staroń, R. Kurczab, D. Warszycki, G. Satała, M. Krawczyk, R. Bugno, T. Lenda, P. Popik, A.S. Hogendorf, A. Hogendorf, K. Dubiel, M. Matłoka, R. Moszczyński-Pętkowski, J. Pieczykolan, M. Wieczorek, P. Zajdel, A.J. Bojarski, Virtual screening-driven discovery of dual 5-HT_6/5-HT_{2A} receptor ligands with pro-cognitive properties, Eur. J. Med. Chem. 185 (2019), https://doi.org/10.1016/j.ejmech.2019.111857.

[22] M.L. Bolognesi, A. Cavalli, Multitarget drug discovery and polypharmacology, ChemMedChem 11 (2016) 1190–1192, https://doi.org/10.1002/cmdc.201600161.

[23] D. Łażewska, R. Kurczab, M. Więcek, K. Kamińska, G. Satała, M. Jastrzębska-Więsek, A. Partyka, A.J. Bojarski, A. Wesołowska, K. Kieć-Kononowicz, J. Handzlik, The computer-aided discovery of novel family of the 5-HT_6 serotonin receptor ligands among derivatives of 4-benzyl-1,3,5-triazine, Eur. J. Med. Chem. 135 (2017) 117–124, https://doi.org/10.1016/j.ejmech.2017.04.033.

[24] R. Kurczab, W. Ali, D. Łażewska, M. Kotańska, M. Jastrzębska-Więsek, G. Satała, M. Więcek, A. Lubelska, G. Latacz, A. Partyka, M. Starek, M. Dąbrowska, A. Wesołowska, C. Jacob, K. Kieć-Kononowicz, J. Handzlik, Computer-aided studies for novel arylhydantoin 1,3,5-triazine derivatives as 5-HT_6 serotonin receptor ligands with antidepressive-like, anxiolytic and antiobesity action in vivo, Molecules 23 (2018) 1–26, https://doi.org/10.3390/molecules23102529.

[25] W. Ali, M. Więcek, D. Łażewska, R. Kurczab, M. Jastrzębska-Więsek, G. Satała, K. Kucwaj-Brysz, A. Lubelska, M. Głuch-Lutwin, B. Mordyl, A. Siwek, M.J. Nasim, A. Partyka, S. Sudoł, G. Latacz, A. Wesołowska, K. Kieć-Kononowicz, J. Handzlik, Synthesis and computer-aided SAR studies for derivatives of phenoxyalkyl-1,3,5-triazine as the new potent ligands for serotonin receptors 5-HT_6, Eur. J. Med. Chem. 178 (2019) 740–751, https://doi.org/10.1016/j.ejmech.2019.06.022.

[26] S. Sudoł, K. Kucwaj-Brysz, R. Kurczab, N. Wilczyńska, M. Jastrzębska-Więsek, G. Satała, G. Latacza, M. Głuch-Lutwin, B. Mordyl, E. Żesławska, W. Nitek, A. Partyka, K. Buzun, A. Doroz-Płonka, A. Wesołowska, A. Bielawska, J. Handzlik, Chlorine substituents- and linker topology as factors for 5-HT_6R activity of novel highly active 1,3,5-triazine derivatives with procognitive properties in vivo, Eur. J. Med. Chem. 203 (2020), 112529, https://doi.org/10.1016/j.ejmech.2020.112529.

[27] S. Sudoł, A. Cios, M. Jastrzębska-Więsek, E. Honkisz-Orzechowska, B. Mordyl, N. Wilczyńska-Zawal, G. Satała, K. Kucwaj-Brysz, A. Partyka, G. Latacz, A. Olejarz-Maciej, A. Wesołowska, J. Handzlik, The phenoxyalkyltriazine antagonists for 5-HT_6 receptor with promising procognitive and pharmacokinetic properties in vivo in search for a novel therapeutic approach to dementia diseases, Int. J. Mol. Sci. 22 (2021), https://doi.org/10.3390/ijms221910773.

[28] A. Chatterjee, S.J. Cutler, R.J. Doerksen, I.A. Khanb, J.S. Williamson, Discovery of thienoquinolone derivatives as selective and ATP non-competitive CDK5/p25 inhibitors by structure-based virtual screening, Bioorg. Med. Chem. 23 (2008) 1–7, https://doi.org/10.1038/jid.2014.371.

[29] G.H. Kuo, A. DeAngelis, S. Emanuel, A. Wang, Y. Zhang, P.J. Connolly, X. Chen, R. H. Gruninger, C. Rugg, A. Fuentes-Pesquera, S.A. Middleton, L. Jolliffe, W. V. Murray, Synthesis and identification of [1,3,5]triazine-pyridine biheteroaryl as a novel series of potent cyclin-dependent kinase inhibitors, J. Med. Chem. 48 (2005) 4535–4546, https://doi.org/10.1021/jm040214h.

[30] E. Jameel, P. Meena, M. Maqbool, J. Kumar, W. Ahmed, S. Mumtazuddin, M. Tiwari, N. Hoda, B. Jayaram, Rational design, synthesis and biological screening of triazine-triazolopyrimidine hybrids as multitarget anti-Alzheimer agents, Eur. J. Med. Chem. 136 (2017) 36–51, https://doi.org/10.1016/j.ejmech.2017.04.064.

[31] A.J. Veloso, A.M. Chow, D. Dhar, D.W.F. Tang, H.V.S. Ganesh, S. Mikhaylichenko, I.R. Brown, K. Kerman, Biological activity of sym-triazines with acetylcholine-like substitutions as multitarget modulators of Alzheimer's disease, ACS Chem. Neurosci. 4 (2013) 924–929, https://doi.org/10.1021/cn400028w.

[32] M. Maqbool, A. Manral, E. Jameel, J. Kumar, V. Saini, A. Shandilya, M. Tiwari, N. Hoda, B. Jayaram, Development of cyanopyridine-triazine hybrids as lead multitarget anti-Alzheimer agents, Bioorg. Med. Chem. 24 (2016) 2777–2788, https://doi.org/10.1016/j.bmc.2016.04.041.

[33] S.N. Khattab, H.H. Khalil, A.A. Bekhit, M.M.A. El-Rahman, A. El-Faham, F. Albericio, Synthesis and preliminary biological evaluation of 1,3,5-triazine amino acid derivatives to study their MAO inhibitors, Molecules 20 (2015), 15976, https://doi.org/10.3390/molecules200915976. –15988.

[34] D. Łażewska, A. Olejarz-Maciej, M. Kaleta, M. Bajda, A. Siwek, T. Karcz, A. Doroz-Płonka, U. Cichoń, K. Kuder, K. Kieć-Kononowicz, 4-tert-Pentylphenoxyalkyl derivatives - histamine H3 receptor ligands and monoamine oxidase B inhibitors, Bioorg. Med. Chem. Lett. 28 (2018) 3596–3600, https://doi.org/10.1016/J.BMCL.2018.10.048.

[35] V. Sharma, M. Gupta, Designing of kinase hinge binders: a medicinal chemistry perspective, Chem. Biol. Drug Des. 100 (2022), https://doi.org/10.1111/CBDD.14024.

[36] Q. Deveuve, V. Gouilleux-Gruart, G. Thibault, L. Lajoie, [The hinge region of therapeutic antibodies: major importance of a short sequence], Med. Sci. 35 (2019) 1098–1099, https://doi.org/10.1051/MEDSCI/2019218.

[37] A. Zeb, D. Kim, S.I. Alam, M. Son, R. Kumar, S. Rampogu, S. Parameswaran, R. M. Shelake, R.M. Rana, S. Parate, J.-Y. Kim, K.W. Lee, Computational simulations identify pyrrolidine-2,3-dione derivatives as novel inhibitors of CDK5/p25 complex to attenuate alzheimer's pathology, J. Clin. Med. 8 (2019) 746, https://doi.org/10.3390/jcm8050746.

[38] J.S. Ahn, M.L. Radhakrishnan, M. Mapelli, S. Choi, B. Tidor, G.D. Cuny, A. Musacchio, L.A. Yeh, K.S. Kosik, Defining CDK5 ligand chemical space with small molecule inhibitors of tau phosphorylation, Chem. Biol. 12 (2005) 811–823, https://doi.org/10.1016/j.chembiol.2005.05.011.

[39] J. Liu, J. Yang, Y. Xu, G. Guo, L. Cai, H. Wu, Y. Zhao, X. Zhang, Roscovitine, a CDK5 inhibitor, alleviates sevoflurane-induced cognitive dysfunction via regulation tau/GSK3β and ERK/PPARγ/CREB signaling, Cell. Physiol. Biochem. 44 (2017) 423–435, https://doi.org/10.1159/000485008.

[40] A. Lubelska, G. Latacz, M. Jastrzębska-Więsek, M. Kotańska, R. Kurczab, A. Partyka, M.A. Marć, D. Wilczyńska, A. Doroz-Płonka, D. Łażewska, A. Wesołowska, K. Kieć-Kononowicz, J. Handzlik, Are the hydantoin-1,3,5-triazine 5-HT_6R ligands a hope to a find new procognitive and anti-obesity drug? Considerations based on primary in vivo assays and ADME-tox profile in vitro, Molecules 24 (2019), https://doi.org/10.3390/MOLECULES24244472.

[41] G. Latacz, A. Lubelska, M. Jastrzębska-Więsek, A. Partyka, M.A. Marć, G. Satała, D. Wilczyńska, M. Kotańska, M. Więcek, K. Kamińska, A. Wesołowska, K. Kieć-Kononowicz, J. Handzlik, The 1,3,5-triazine derivatives as innovative chemical family of 5-HT6 serotonin receptor agents with therapeutic perspectives for cognitive impairment, Int. J. Mol. Sci. 20 (2019), https://doi.org/10.3390/ijms20143420.

[42] S. Swallow, Fluorine in medicinal chemistry, in: Progress in Medicinal Chemistry, first ed., Elsevier B.V., 2015 https://doi.org/10.1016/bs.pmch.2014.11.001.

[43] A. Vulpetti, C. Dalvit, Hydrogen bond acceptor propensity of different fluorine atom types: an analysis of experimentally and computationally derived parameters, Chem. Eur J. 27 (2021) 8764–8773, https://doi.org/10.1002/chem.202100301.

[44] E. Szymańska, A. Drabczyńska, T. Karcz, C.E. Müller, M. Köse, J. Karolak-Wojciechowska, A. Fruziński, J. Schabikowski, A. Doroz-Płonka, J. Handzlik, K. Kieć-Kononowicz, Similarities and differences in affinity and binding modes of tricyclic pyrimido- and pyrazinoxanthines at human and rat adenosine receptors, Bioorg. Med. Chem. 24 (2016) 4347–4362, https://doi.org/10.1016/J.BMC.2016.07.028.

[45] X. Chen, A. Murawski, K. Patel, C.L. Crespi, P.V. Balimane, A novel design of artificial membrane for improving the PAMPA model, Pharm. Res. (N. Y.) 25 (2008) 1511–1520, https://doi.org/10.1007/s11095-007-9517-8.

[46] J. Śniecikowska, M. Głuch-Lutwin, A. Bucki, A. Więckowska, A. Siwek, M. Jastrzębska-Więsek, A. Partyka, D. Wilczyńska, K. Pytka, G. Latacz, K. Przejczowska-Pomierny, E. Wyska, A. Wesołowska, M. Pawłowski, A. Newman-Tancredi, M. Kołaczkowski M, Discovery of novel pERK1/2- or β-arrestin-preferring 5-HT_{1A} receptor-biased agonists: diversified therapeutic-like versus side effect profile, J. Med. Chem. 63 (2020) 10946–10971. https://reference.medscape.com/medline/abstract/32883072. (Accessed 1 December 2021).

[47] T. Nagatomo, M. Rashid, H. Abul Muntasir, T. Komiyama, Functions of 5-HT_{2A} receptor and its antagonists in the cardiovascular system, Pharmacol. Ther. 104 (2004) 59–81, https://doi.org/10.1016/J.PHARMTHERA.2004.08.005.

[48] K. Yamada, H. Niki, H. Nagai, M. Nishikawa, H. Nakagawa, Serotonin potentiates high-glucose-induced endothelial injury: the role of serotonin and 5-HT_{2A} receptors in promoting thrombosis in diabetes, J. Pharmacol. Sci. 119 (2012) 243–250, https://doi.org/10.1254/JPHS.12009FP.

[49] S.B. Floresco, J.D. Jentsch, Pharmacological enhancement of memory and executive functioning in laboratory animals, Neuropsychopharmacology 36 (2011) 227–250, https://doi.org/10.1038/NPP.2010.158.

[50] K.C.F. Fone, An update on the role of the 5-hydroxytryptamine6 receptor in cognitive function, Neuropharmacology 55 (2008) 1015–1022, https://doi.org/10.1016/J.NEUROPHARM.2008.06.061.

[51] F.J. van der Staay, K. Rutten, C. Erb, A. Blokland, Effects of the cognition impairer MK-801 on learning and memory in mice and rats, Behav. Brain Res. 220 (2011) 215–229, https://doi.org/10.1016/J.BBR.2011.01.052.

[52] H.Y. Meltzer, L. Rajagopal, M. Hung, Y. Oyamada, S. Kwon, M. Horiguchi, Translating the N-methyl-D-aspartate receptor antagonist model of schizophrenia to treatments for cognitive impairment in schizophrenia, Int. J. Neuropsychopharmacol. 16 (2013) 2181–2194, https://doi.org/10.1017/S1461145713000928.

[53] A. Nair, S. Jacob, A simple practice guide for dose conversion between animals and human, J. Basic Clin. Pharm. 7 (2016) 27, https://doi.org/10.4103/0976-0105.177703.

[54] G.M. Sheldrick, Foundations and Advances SHELXT-Integrated space-group and crystal-structure determination, Acta Crystallogr. 71 (2015) 3–8, https://doi.org/10.1107/S2053273314026370.

[55] G.M. Sheldrick, Crystal structure refinement with SHELXL, Acta Crystallogr., Sect. C: Struct. Chem. 71 (2015) 3–8, https://doi.org/10.1107/S2053229614024218.

[56] C.F. MacRae, I. Sovago, S.J. Cottrell, P.T.A. Galek, P. McCabe, E. Pidcock, M. Platings, G.P. Shields, J.S. Stevens, M. Towler, P.A. Wood, Mercury 4.0: from visualization to analysis, design and prediction, J. Appl. Crystallogr. 53 (2020) 226–235, https://doi.org/10.1107/S1600576719014092.

[57] C. Yung-Chi, W.H. Prusoff, Relationship between the inhibition constant (K1) and the concentration of inhibitor which causes 50 per cent inhibition (I50) of an enzymatic reaction, Biochem. Pharmacol. 22 (1973) 3099–3108, https://doi.org/10.1016/0006-2952(73)90196-2.

[58] P. Corporation, Using the Kinase Enzyme Systems with the ADP-GloTM Assay Technical Manual, TM553, (n.d.). www.promega.com (accessed November 24, 2021).
[59] A. Ennaceur, J. Delacour, A new one-trial test for neurobiological studies of memory in rats. 1: behavioral data, Behav, Brain Res. 31 (1988) 47–59, https://doi.org/10.1016/0166-4328(88)90157-X.
[60] P. Zajdel, T. Kos, K. Marciniec, G. Satała, V. Canale, K. Kamiński, M. Hołuj, T. Lenda, R. Koralewski, M. Bednarski, L. Nowiński, J. Wójcikowski, W.A. Daniel, A. Nikiforuk, I. Nalepa, P. Chmielarz, J. Kuśmierczyk, A.J. Bojarski, P. Popik, Novel multi-target azinesulfonamides of cyclic amine derivatives as potential antipsychotics with pro-social and pro-cognitive effects, Eur. J. Med. Chem. 145 (2018) 790–804, https://doi.org/10.1016/J.EJMECH.2018.01.002.
[61] J. Rychtyk, A. Partyka, J. Gdula-Argasińska, K. Mysłowska, N. Wilczyńska, M. Jastrzębska-Więsek, A. Wesołowska, 5-HT6 receptor agonist and antagonist improve memory impairments and hippocampal BDNF signaling alterations induced by MK-801, Brain Res. 1722 (2019), https://doi.org/10.1016/j.brainres.2019.146375.
[62] R.D. Porsolt, A. Bertin, M. Jalfre, Behavioural despair" in rats and mice: strain differences and the effects of imipramine, Eur. J. Pharmacol. 51 (1978) 291–294, https://doi.org/10.1016/0014-2999(78)90414-4.
[63] S. Pellow, S.E. File, Anxiolytic and anxiogenic drug effects on exploratory activity in an elevated plus-maze: a novel test of anxiety in the rat, Pharmacol. Biochem. Behav. 24 (1986) 525–529, https://doi.org/10.1016/0091-3057(86)90552-6.